Review | Open Access

AI Agent

Yu et al. AI Agent 2026, 2, 32 DOI:10.20517/aiagent.2026.24

Unveiling catalytic microenvironments: the convergence of conventional computations and machine learning paradigms

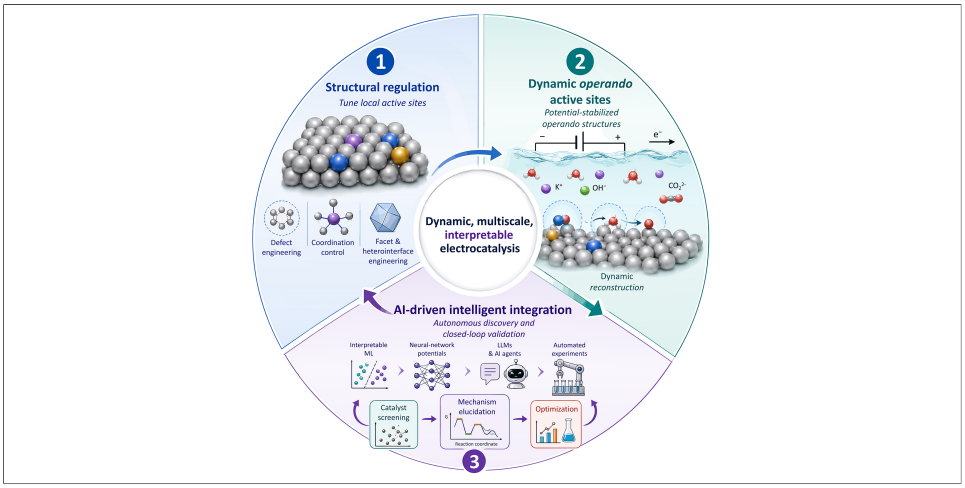
Xiansheng Yu[1,2], Letian Chen[3], Xu Hu[3], Fengjuan Chen[1], Xu Zhang[2], Zhen Zhou[4]

Keywords:
Electrocatalysis, dynamic active sites, grand-canonical density functional theory, machine learning, AI agents

Citation: Yu, X.; Chen, L.; Hu, X.; Chen, F.; Zhang, X.; Zhou, Z. Unveiling catalytic microenvironments: the convergence of conventional computations and machine learning paradigms. *AI Agent* **2026**, *2*, 32. https://dx.doi.org/10.20517/aiagent.2026.24

Received: 10 Jun 2026
First Decision: 24 Aug 2026
Revised: 30 Sep 2026
Accepted: 14 Oct 2026
Published: 6 Nov 2026

Academic Editor:
Hao Li
Copy Editor:
Tong Wang
Production Editor:
Tong Wang



Abstract

Electrocatalysis is central to energy conversion and chemical transformations needed for carbon neutrality. Yet static structural models remain common for rationalizing catalytic performance, despite growing evidence that activity depends on dynamic active-site microenvironments. In this Review, we synthesize recent advances from three connected perspectives. First, we examine structural regulation strategies, including defect engineering, coordination engineering, crystal-facet control and heterointerface construction. These approaches tune local coordination environments, electronic structures and intermediate adsorption, thereby lowering reaction barriers and reshaping catalytic pathways. Second, we highlight grand-canonical density functional theory, constant-potential molecular dynamics and explicit interfacial simulations. These methods

[1]Key Laboratory of Solid State Physics and Devices Autonomous Region, School of Materials Science & Engineering, Xinjiang University, Urumqi 830046, Xinjiang, China.
[2]Interdisciplinary Research Center for Sustainable Energy Science and Engineering (IRC4SE[2]), School of Chemical Engineering, Zhengzhou University, Zhengzhou 450001, Henan, China.
[3]School of Materials Science and Engineering, Institute of New Energy Material Chemistry, Renewable Energy Conversion and Storage Center (ReCast), Key Laboratory of Advanced Energy Materials Chemistry (Ministry of Education), Nankai University, Tianjin 300350, China.
[4]College of New Energy and Intelligent Manufacturing, Henan University, Zhengzhou 450046, China.

Correspondence to: Prof. Fengjuan Chen, Key Laboratory of Solid State Physics and Devices Autonomous Region, School of Materials Science & Engineering, Xinjiang University, Urumqi 830046, Xinjiang, China. E-mail: fjchen@xju.edu.cn; Prof. Xu Zhang, Interdisciplinary Research Center for Sustainable Energy Science and Engineering (IRC4SE[2]), School of Chemical Engineering, Zhengzhou University, Zhengzhou 450001, Henan, China. E-mail: zzuzhangxu@zzu.edu.cn

show how applied potential, electrolyte composition, solvation structure and surface reconstruction jointly determine operando active-site configurations. They further suggest that true active sites often arise as potential-stabilized, dynamically reconstructed states rather than idealized as-prepared structures. Third, interpretable machine learning and symbolic regression are emerging as tools for identifying physically meaningful descriptors that connect local structural and electronic microenvironments with catalytic activity. In parallel, neural network potentials extend atomistic simulations to the spatial and temporal scales needed to resolve evolving interfacial microenvironments. Large language models, AI agents and automated laboratories further create opportunities to integrate heterogeneous mechanistic knowledge with simulations and experimental feedback. By linking rational structural design, operando analysis and data-driven automation, these advances are moving electrocatalysis beyond empirical trial-and-error toward microenvironment-informed, mechanism-guided discovery under realistic reaction conditions.

INTRODUCTION

Against the backdrop of the global energy transition and the pursuit of carbon neutrality[1,2], electrocatalysis has become a major frontier in energy and chemical research. By using electrical energy to drive chemical reactions, electrocatalysis enables green, efficient and highly tunable routes for energy conversion and chemical transformation[3-5]. Electrocatalysts are central to this process because they lower reaction activation barriers[6], regulate intermediate adsorption[7], optimize electron-transfer pathways[8], and improve product selectivity[9]. Therefore, identifying the origin of electrocatalytic activity and using this knowledge to design high-performance catalytic materials remain central challenges in the field.

Current research on electrocatalysts remains largely centered on developing high-performance materials. Their catalytic behavior is typically assessed using macroscopic metrics, including overpotential, half-wave potential, current density, stability and Faradaic efficiency[10,11]. Although these material-level properties are important, they offer limited insight into the microscopic origins of catalytic activity. Advances in operando characterization and computational methods now show that electrocatalysis is governed not only by bulk material properties, but also by the local environments of surface active sites under realistic reaction conditions[12,13]. In this Review, we define the catalytic microenvironment as the local structural, electronic and interfacial environment surrounding an active site, including its evolution during reaction. This microenvironment includes intrinsic structural factors, such as coordination geometry, defects, exposed facets and heterointerfaces. It also includes condition-dependent factors, including interfacial charge redistribution, electrode potential, electrolyte composition, solvation structure, adsorbate configuration and surface reconstruction. These factors are strongly coupled rather than independent. Structural regulation modifies local electronic structure and intermediate binding, whereas the electrochemical environment can reorganize charge distributions, coordination states and even the identity of the active site. Catalytic activity should therefore be understood as an emergent property of an evolving active-site microenvironment, rather than solely of an idealized static catalyst structure.

At the microscopic scale, the local environment of an active site can be tuned through intrinsic structural motifs, including defects, coordination geometries, exposed facets and heterointerfaces. These structural features redistribute local charge, modulate orbital interactions and alter the adsorption energetics of reaction intermediates. They therefore provide the basis for conventional structure-activity relationships in electrocatalysis. However, the active-site environment under operating conditions can differ substantially from that inferred from the as-prepared catalyst. Applied potential, electrolyte composition, interfacial solvation, adsorbate coverage and surface reconstruction can continuously reconfigure the coordination and electronic states of catalytic centers, giving rise to dynamically evolving operando microenvironments. A comprehensive understanding of catalytic activity therefore requires not only clarifying how intrinsic

structures define local active sites, but also resolving how these sites evolve and function under realistic electrochemical conditions.

However, simulating the dynamic evolution of these interfaces requires access to large spatial and temporal scales, which remains challenging for conventional theoretical methods. Data-driven approaches, particularly machine learning (ML), have therefore emerged as powerful tools for accelerating atomistic simulations and bridging this scale gap. Beyond simulation acceleration, large language models (LLMs), artificial intelligence (AI) agents and automated laboratories are beginning to coordinate increasingly complex computational and experimental workflows. These platforms can integrate knowledge extraction, candidate generation, theoretical evaluation and experimental validation, thereby advancing the field from isolated prediction toward closed-loop catalyst discovery[14,15].

Building on this progression from intrinsic structural regulation to operando evolution and data-driven analysis, this Review examines catalytic microenvironments from three interconnected perspectives. First, it discusses how intrinsic structural characteristics modulate local coordination environments, electronic structures and intermediate adsorption. Second, it examines the dynamic evolution of active sites under external driving forces, with emphasis on operando microenvironments shaped by applied potential, electrolyte composition, interfacial solvation and surface reconstruction. Third, it considers AI as a framework for decoding this multiscale complexity. Particular attention is given to ML and neural network potentials (NNPs), which extend the accessible limits of atomistic simulation, and to LLMs and AI agents, which can coordinate these tools into collaborative semantic-reasoning and atomic-simulation workflows. When integrated with automated experiments, these intelligent systems can support high-throughput screening, mechanistic interpretation, inverse design and closed-loop optimization. Together, these perspectives provide a framework for the rational design of next-generation electrocatalysts under realistic operating conditions and for the development of intelligent discovery workflows.

THE MICROSCOPIC MECHANISM OF THE STRUCTURE ON CATALYTIC ACTIVITY

At the microscopic scale, electrocatalytic activity is rooted in the intrinsic composition and structure of the catalyst. Noble metals, alloys, transition-metal oxides, transition-metal sulfides, carbon-based composites and single-atom catalysts therefore exhibit distinct catalytic behaviors and regulation mechanisms[16]. Catalytic performance, however, is governed not only by the number of active sites. It also depends on whether structural modulation can reshape the local coordination environment, electronic distribution, orbital coupling and adsorption configurations of reaction intermediates. These changes can redirect reaction pathways and lower the energy barrier of the rate-determining step[17]. The *d*-band center theory proposed by Hammer and Norskov provides a foundational framework for interpreting catalytic activity[18]. In this model, the bonding strength between adsorbates and transition-metal surfaces is largely determined by the position of the metal *d*-band relative to the Fermi level (E_f). As illustrated in Figure 1, interaction between adsorbate energy levels and the metal *d*-band splits the states into bonding and antibonding components[19]. When the *d*-band center shifts upward toward E_f, antibonding adsorbate-metal states move closer to, or above, the E_f and become less occupied. The reduced occupation of antibonding states strengthens adsorbate-metal bonding, thereby enhancing surface adsorption.

The *d*-band center is most informative for comparatively well-defined transition-metal surfaces where adsorption is dominated by hybridization between metal *d* states and adsorbate orbitals, and where variations in local coordination and interfacial conditions are limited[21]. Despite its conceptual value, the *d*-band center is not a universal descriptor of catalytic activity. Its predictive power may be reduced for multimetallic or strongly reconstructed surfaces, low-coordination sites and systems dominated by

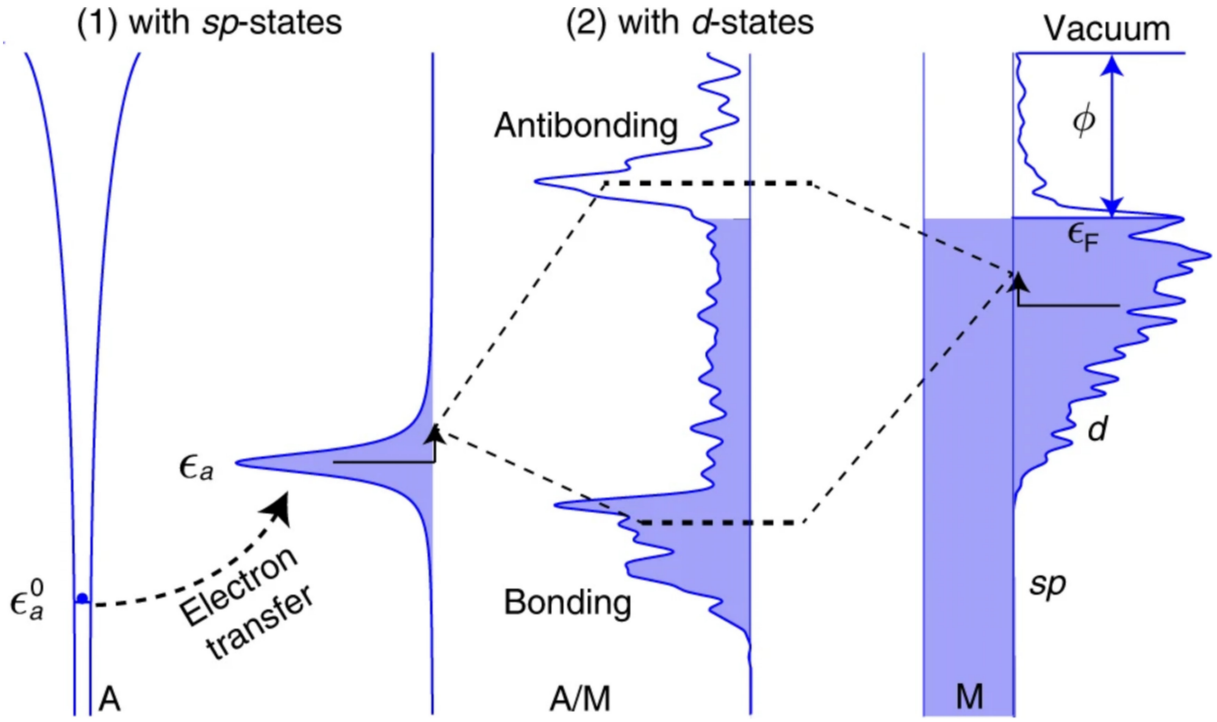


Figure 1. Schematic illustration of adsorbate-metal chemisorption within the d-band reactivity framework[20]. Reproduced from reference[20] under CC BY 4.0 License.

orbital-specific interactions, as well as for electrochemical interfaces where solvation, electric fields and potential-dependent charge redistribution substantially affect adsorption. In complex catalytic microenvironments, adsorption and reaction energetics are jointly shaped by local coordination, orbital hybridization, charge redistribution, spin polarization and interfacial interactions[22,23]. These factors are particularly important in defect-rich catalysts, atomically dispersed active sites and heterointerfaces, where a single energy-averaged descriptor cannot fully capture site-specific electronic interactions. Viewed through this microenvironment framework, structural engineering can be understood as the deliberate regulation of the local atomic and electronic environment around an active site. Defect engineering targets lattice-level imperfections, including vacancies, dopants and distortions. Coordination engineering focuses on the first coordination shell of atomically dispersed active centers, whereas facet and interface engineering tune surface atomic arrangements and interfacial charge redistribution over larger structural length scales[24]. Together, these strategies can modulate the local coordination environment, electronic density of states and surface adsorption behavior, thereby redirecting electrocatalytic reaction pathways and improving catalytic efficiency[25,26]. In the following sections, we discuss the microscopic mechanisms by which defect, coordination, facet and interface engineering regulate electrocatalytic activity.

Defect engineering enables the intrinsic physicochemical properties of catalytic materials to be regulated at the atomic and electronic scales. By controllably introducing zero-dimensional point defects, including vacancies, dopant atoms and lattice distortions, the periodic symmetry of an ideal crystal lattice can be disrupted, thereby tuning catalytic activity[27]. Wang *et al.* constructed charge-polarized Se vacancies in $NiSe_2$ through a sequential phase-conversion and annealing strategy[28]. Electron paramagnetic resonance (EPR) and X-ray photoelectron spectroscopy (XPS) analyses confirmed the formation of electron-trapped Se vacancies and revealed a decrease in the oxidation state of neighboring Ni sites[28]. *In situ* Raman measurements further identified reversible OOH adsorption on the active Ni sites during the $2e^-$ oxygen

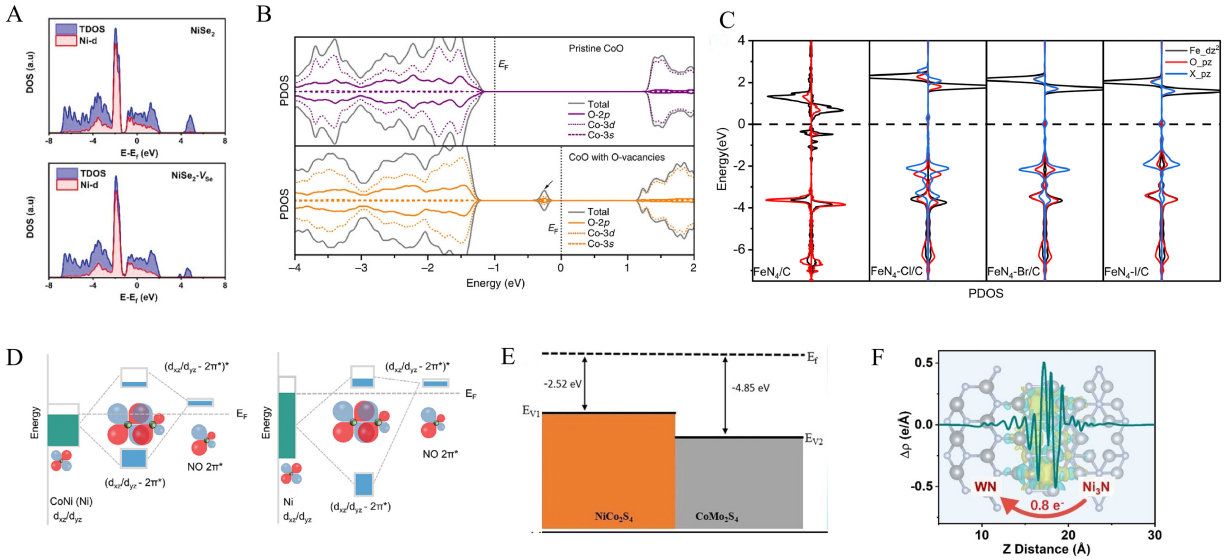


Figure 2. Effect of material structure on catalytic activity. (A) Electronic-structure modulation induced by Se vacancies in $NiSe_2$. Adapted from reference[28] under CC BY license; (B) Vacancy-induced changes in the electronic structure of CoO. Adapted from reference[29] under CC BY 4.0 License; (C) Axial halogen ligands compete with oxygen-containing intermediates for the Fe dz² orbital. Reproduced with permission from reference[33]. Copyright © 2026, Royal Society of Chemistry; (D) Schematic illustration of orbital interactions between the NO 2π^* antibonding orbital and the Ni 3dxz/3dyz orbitals in Ni_1-NC and Co_1Ni_1-NC. Reproduced with permission from reference[34]. Copyright © 2024, Wiley-VCH GmbH; (E) Directional charge transfer at the $NiCo_2S_4/CoMo_2S_4$ heterojunction interface forms highly localized electrophilic and nucleophilic regions. Reproduced with permission from reference[39]. Copyright © 2025, Wiley-VCH GmbH; (F) Interfacial charge redistribution in the WN/Ni_3N heterostructure. Adapted with permission from reference[40]. Copyright © 2024, Wiley-VCH GmbH. DOS: Density of states; TDOS: total density of states; PDOS: projected density of states.

reduction reaction (ORR)[28]. Density functional theory (DFT) calculations showed that the introduction of Se vacancies upshifted the Ni *d*-band center from -1.815 to -1.790 eV, thereby regulating the interaction between Ni active sites and oxygenated intermediates [Figure 2A]. The resulting charge localization strengthened OOH adsorption and brought its adsorption free energy closer to the optimal value, ultimately promoting the selective 2e⁻ ORR pathway toward H_2O_2. Ling *et al.*[29] engineered oxygen-vacancy-rich O-terminated {111} nanofacets on single-crystalline CoO nanorods. X-ray absorption near-edge structure (XANES) and XPS analyses revealed that the introduction of oxygen vacancies induced electron transfer toward the Co *d* states, thereby modifying the local electronic environment of the surface Co sites[29]. DFT calculations further showed that oxygen vacancies generated new electronic states near the E_f through hybridization among O 2*p*, Co 3*d*, and Co 3*s* orbitals [Figure 2B]. These defect-induced electronic states strengthened the adsorption of oxygen-containing intermediates and optimized the adsorption-desorption energetics of OOH, O, and OH*, thereby enhancing both oxygen reduction and oxygen evolution activities.

Coordination engineering enables local charge density at active sites to be precisely tailored by regulating the coordination environment of central metal atoms. Key variables include coordination number, the electronegativity of coordinating heteroatoms, spatial geometry and the incorporation of vacancy defects[30,31]. Unlike defect engineering, which mainly exploits lattice vacancies and unsaturated sites, coordination engineering operates within the first coordination shell. It determines not only whether a site is coordinatively unsaturated, but also which atoms constitute the coordination sphere, how they are spatially arranged and how they electronically couple to the metal center. With the rapid development of single- and dual-atom catalytic systems, such atomically precise control has become a central strategy for tuning active-site reactivity[32]. Luo *et al.*[33] introduced axial halide ligands into 3d transition-metal-nitrogen-carbon (3d TM-N-C) single-atom catalysts, significantly enhancing both structural stability and ORR activity. In Fe-based single-atom systems, the axial halide ligands electronically compete with oxygen-containing

intermediates for the Fe dz^2 orbital [Figure 2C]. This orbital competition weakens the overly strong Fe-O interaction, thereby shifting the active site closer to the apex of the volcano plot. As a result, the limiting potential reached 0.96 V, surpassing that of conventional Pt-based benchmarks. The concept of coordination engineering has also been extended to dual-atom catalysts, where long-range electronic effects and intermetallic orbital coupling become important for activating stable small molecules. In a Co-Ni dual-atom catalyst embedded in a nitrogen-doped hollow carbon matrix, Co-Ni *d*-*d* orbital coupling induces pronounced electron enrichment at the Ni site[34]. This synergistic effect shifts the Ni *d*-band center upward toward the E_f, promoting electron transfer from the Ni 3dxz/3dyz orbitals to the $2\pi^*$ antibonding orbital of adsorbed NO [Figure 2D]. This interaction weakens the N-O bond and markedly accelerates both NO adsorption and electrocatalytic oxidation.

Different exposed crystal facets differ markedly in atomic stacking sequence, coordination number and dangling-bond density. These facet-dependent features directly influence the adsorption free energies of reactants and key intermediates on different crystal planes[35]. Through oriented synthesis, selectively exposing high-energy facets or facets enriched with low-coordination atoms can optimize adsorption-desorption behavior during electrochemical reactions. This strategy thereby enhances the intrinsic catalytic activity of the material. Beyond facet regulation, heterostructure construction has emerged as an important interfacial engineering strategy for overcoming the thermodynamic limitations of single-component electrocatalysts[36]. When materials with different work functions or electronic structures form a heterointerface, Fermi-level equilibration can induce interfacial charge redistribution and generate a built-in electric field[37,38]. Such heterointerfacial interactions not only redistribute charge at active centers, shifting the *d*-band center and optimizing local charge density, but also create diverse active sites through synergistic coupling between different components. This effect is particularly beneficial for complex multistep proton-coupled electron-transfer reactions, because it can help break linear scaling relationships between intermediate adsorption energies. Nwaji *et al.* synthesized a $NiCo_2S_4/CoMo_2S_4$ heterojunction system[39]. As illustrated in Figure 2E, electrons spontaneously migrate from lower-work-function $NiCo_2S_4$ to $CoMo_2S_4$ to equilibrate the E_f. This directional charge migration creates highly localized electrophilic and nucleophilic regions at the interface. The polarized heterointerface preferentially adsorbs the carbonyl and amino groups at the electrophilic region of $NiCo_2S_4$ and the nucleophilic region of $CoMo_2S_4$, respectively[39]. This interfacial polarization promotes C-N bond stretching and cleavage in the urea molecular framework, substantially lowers the free-energy change of the rate-determining step, and accelerates the complete decomposition of urea into CO_2 and N_2. Yang *et al.*[40] constructed a metallic WN-Ni_3N heterostructure to regulate the local electronic environment of interfacial active sites. Differential charge-density and Bader charge analyses revealed pronounced electron redistribution across the heterointerface, with approximately 0.8 e transferred from Ni_3N to WN and electron accumulation at W sites near the interface [Figure 2F]. DFT calculations further showed that this interfacial electronic reconstruction weakened both H 1*s*-W *d* and O 2*p*-W *d* interactions compared with pristine WN, thereby optimizing the binding strengths of H and OH intermediates. As a result, the heterostructure promoted OH* removal and H_2 release while maintaining favorable hydrogen adsorption, leading to accelerated alkaline hydrogen-evolution kinetics.

THE MICROSCOPIC MECHANISM OF THE CATALYST UNDER REALISTIC WORKING CONDITIONS

Electrocatalytic reactions are intrinsically complex heterogeneous processes at solid-liquid interfaces. They involve reactant adsorption, multistep proton-coupled electron transfer (PCET)[41], intermediate evolution and product desorption. During these microscopic processes, the dynamic restructuring of surface active sites and the evolution of their local coordination environments jointly determine macroscopic catalytic performance[42]. With advances in computational chemistry and operando characterization, it has become

increasingly clear that conventional constant-charge models cannot fully describe realistic electrochemical interfaces. Recent studies show that grand-canonical density functional theory (GC-DFT)[43] and constant-potential molecular dynamics (CP-MD)[44,45] can more faithfully capture the effect of electrode potential on catalytic systems. These approaches therefore provide a more realistic framework for describing electrocatalytic processes under working conditions[46].

Here, it is useful to distinguish the terms "grand-canonical" and "constant-potential". Grand-canonical refers to a thermodynamic ensemble in which the electron chemical potential is fixed, while the electron number can fluctuate through exchange with an electron reservoir[47]. By contrast, constant-potential describes an electrochemical condition or simulation protocol in which the electrode potential is maintained at a prescribed value[48]. GC-DFT therefore provides a formally grand-canonical framework for electronic-structure calculations at constant electrode potential, but the two terms are not interchangeable. Some constant-potential schemes maintain or approximate a target electrode potential through iterative charge adjustment, fluctuating-charge algorithms or potential-dependent models, without rigorously sampling the full electronic grand-canonical ensemble. In the following discussion, we use "grand-canonical" specifically to denote the underlying thermodynamic ensemble, and "constant-potential" more broadly to describe methods or simulations that impose or maintain a prescribed electrode potential.

Electrode potential is not merely a thermodynamic descriptor in electrocatalysis, but an active driving force that reshapes interfacial electronic structures, adsorption configurations and catalytic microenvironments[49,50]. For decades, theoretical studies of electrocatalysis have commonly used constant-charge surface models to represent electrode-electrolyte interfaces[51]. Although these models have advanced the understanding of reaction pathways, adsorption-energy scaling relationships and rate-determining steps, they impose a fixed surface charge. They therefore cannot explicitly describe dynamic charge exchange between the electrode and electrolyte under applied potentials. This limitation makes it difficult to capture potential-induced charge redistribution, adsorbate dipole responses, adsorption-configuration changes and electric-double-layer restructuring. As a result, constant-charge models often provide an incomplete description of potential effects, pH-dependent interfacial behavior and the true nature of active sites under realistic operating conditions. Yang *et al.* employed DFT calculations and surface Pourbaix diagrams to investigate the potential- and pH-dependent surface states of dual-atom catalysts (DACs)[52]. Their analysis of eight homonuclear and 64 heteronuclear DACs revealed that adsorbate-covered configurations are often more stable than pristine structures. As shown in Figure 3A, Fe-Ni-C maintains a pristine surface between -0.36 and 0.28 V *vs.* standard hydrogen electrode (SHE) at pH = 0, whereas Fe-Ni-$N_{1,2,4}$-C favors H*- or O*-covered states. At -0.35 V *vs.* SHE, Fe-Ni-C remains pristine while Fe-Ni-$N_{1,2,4}$-C becomes H*-covered. These findings demonstrate that electrode potential, pH and local coordination jointly determine stable active-site configurations under electrochemical conditions. Li *et al.* employed a fully converged constant-potential grand-canonical framework[53] coupled with the VASPsol implicit solvation model[54] to investigate the two-electron ORR on Pd-O_3 single-atom sites. By comparing Pd-O_3 motifs embedded in planar and curved carbon environments, they found that surface curvature induces a localized tip-enhanced electric field around the out-of-plane Pd center. As shown in Figure 3B, the dipole moment of adsorbed O_2 on the curved Pd-O_3 site increased markedly as the applied potential shifted negatively from 0.7 to 0.1 V. By contrast, O_2 on the planar site showed a much smaller dipole moment that was nearly independent of potential. This potential-dependent polarization promoted O_2 activation and facilitated formation of the key OOH intermediate, thereby enhancing selective H_2O_2 electrosynthesis. Liu *et al.* further showed that electrode potential and pH can jointly reshape reaction thermodynamics by modulating intermediate adsorption[55]. Using constant-potential first-principles calculations for a two-dimensional FeCl organometallic framework, they established potential-dependent energetics for key ORR/oxygen evolution reaction (OER) intermediates by systematically varying the surface charge. The adsorption of OOH, O and OH* responded differently to

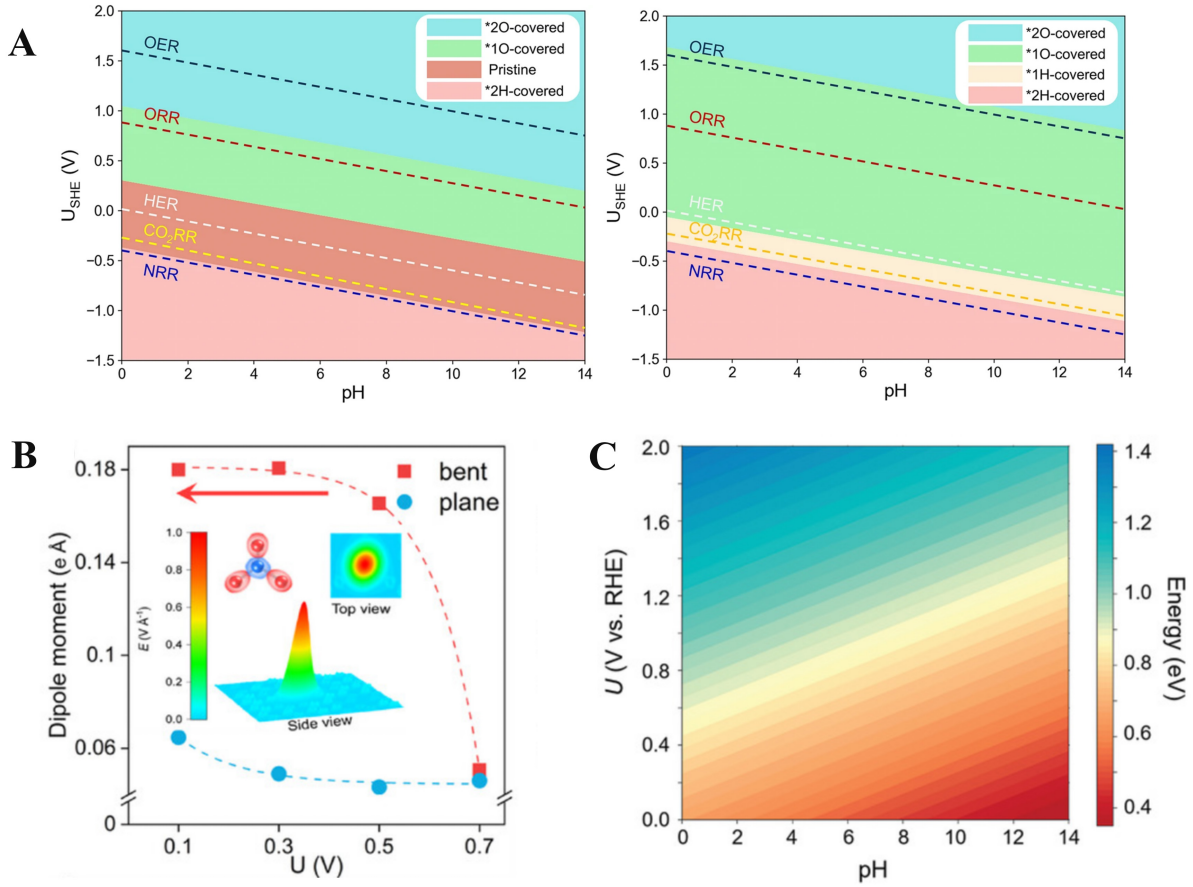


Figure 3. Effect of applied potential on catalytic activity. (A) Potential- and pH-dependent surface Pourbaix diagrams of Fe-Ni-C and Fe-Ni-$N_{1,2,4}$-C dual-atom catalysts. Reproduced from reference[52] under CC BY 4.0 License; (B) Potential-dependent O_2 polarization on bent and planar Pd-O_3 sites together with the localized electric-field distribution at the curved Pd-O_3 site. Adapted from reference[53] under Creative Commons Attribution License; (C) Potential- and pH-dependent OH adsorption energetics on the FeCl monolayer. Adapted with permission from reference[55]. Copyright © 2022, Wiley-VCH GmbH. OER: Oxygen evolution reaction; ORR: oxygen reduction reaction; HER: hydrogen evolution reaction; NRR: nitrogen reduction reaction; RHE: reversible hydrogen electrode.

electrochemical conditions, leading to changes in the potential-determining steps and bifunctional activity between acidic and alkaline media. As shown in Figure 3C, the OH* adsorption energy evolved continuously across the potential-pH space, highlighting the dynamic coupling between the electrochemical environment and intermediate stability. These results indicate that applied potential can reshape the local electronic microenvironment not only by changing surface charge, but also by modulating interfacial electric fields and adsorbate polarization.

CP-MD maintains the electrode at a prescribed potential during the simulation while allowing charges on electrode atoms to polarize and self-consistently adjust as the interfacial microstructure evolves. This treatment more closely approximates experimental constant-potential conditions and provides a more realistic description of the coupling among solvent orientation, electrolyte-ion distribution and electrode surface charge[56,57]. CP-MD therefore enables atomistic insight into how applied potential reshapes the local solvation environment, modulates the adsorption stability of key intermediates and changes reaction barriers. It provides a mechanistic framework for understanding how complex external environments synergistically regulate catalytic activity.

CP-MD studies have shown that electrolyte ions are not inert spectators, but can directly regulate catalytic activity by reshaping interfacial hydrogen-bond networks and water activation processes[58,59]. Chen *et al.*[60] used CP-MD to examine how surface terminations regulate the interfacial hydrogen-bond network and proton-coupled electron-transfer kinetics on Ti_2C MXenes. By comparing O-terminated and mixed O/OH-terminated surfaces, they found that surface hydroxyl groups draw interfacial water closer to the electrode and reorganize the electric double layer into a more continuous hydrogen-bond network. As shown in Figure 4A, OH terminations reduced the water-surface separation by approximately 0.4 Å, acting as hydrogen-bond anchors that enhanced interfacial water connectivity. This restructuring facilitated hydronium dehydration and stabilized proton-transfer intermediates, particularly Zundel cations, thereby lowering the kinetic barriers for the Volmer and Heyrovsky steps. These results indicate that surface chemistry can regulate electrocatalytic kinetics not only through intermediate adsorption energetics, but also by dynamically restructuring the interfacial hydrogen-bond microenvironment. Qin *et al.* combined constant-potential DFT calculations with *ab initio* molecular dynamics simulations to examine the dynamic sintering of Cu single-atom sites in Cu-N-C catalysts during electrochemical CO_2 reduction[61]. Co-adsorbed H and CO weakened Cu-N coordination and promoted the formation of mobile $Cu(CO)_2$ species, thereby facilitating Cu leaching from the initial CuN_4 sites. Constant-potential ab initio molecular dynamics (AIMD) at -1.0 V *vs.* SHE directly captured Cu-N bond cleavage and migration of the detached $Cu(CO)_2$ moiety [Figure 4B]. Subsequent Cu-Cu bond formation with a neighboring Cu site marked the initial stage of Cu sintering under reaction conditions. The resulting Cu clusters further facilitated C-C coupling and contributed to C_2 product formation. These findings indicate that reaction intermediates and applied potential can cooperatively restructure nominally isolated active sites into new catalytic ensembles under operating conditions. Beyond describing interfacial hydrogen-bond restructuring and potential-induced active-site evolution, dynamic simulations have reshaped our understanding of real catalytic structures under operating conditions. In some cases, explicit dynamic interfacial simulations do more than refine static models. They can uncover hidden mechanisms, including intermediate-assisted structural reconstruction, dynamic active-site regeneration and potential-dependent changes in reaction pathways. Using a NiFe-NC core-shell catalyst as a model system, Xue *et al.* combined constant-potential calculations, explicit-solvent AIMD and experimental characterization[62]. They showed that ORR/OER activity and stability do not originate from the static core-shell structure itself, but from dynamic reconstruction during reaction. Metal atoms in the NiFe alloy core can diffuse outward into the nitrogen-doped carbon shell and form M-N-C single-atom sites, among which Fe-N-C shows superior ORR/OER activity[62]. As shown in Figure 4C, explicit-solvent AIMD further revealed the regeneration mechanism of Fe-N-C sites. Once the original central Fe atom dissociates, Fe from the outermost layer of the core can migrate outward with the assistance of OH* and reoccupy the N-coordination site. This process involves only a small free-energy barrier and becomes more favorable under operating potentials. These results indicate that the high stability of core-shell catalysts arises from the continuous replenishment of core metal atoms, which enables active-site regeneration under reaction conditions.

LEVERAGING AN AI-DRIVEN APPROACH TO UNVEIL THE MICROSCOPIC MECHANISMS OF ELECTROCATALYTIC ACTIVITY AND ENABLE THE EFFICIENT SCREENING OF ELECTROCATALYSTS

At the atomic and molecular scales, resolving the microscopic origins of electrocatalytic activity is essential for moving catalyst development from empirical trial-and-error toward rational design. Electrocatalytic mechanisms have traditionally been investigated using advanced operando characterization techniques and DFT calculations. Although operando spectroscopic and microscopic methods have made substantial progress in tracking dynamic reaction processes, their spatiotemporal resolution remains limited. As a result, ultrashort-lived reaction intermediates and transient atomic-scale structural reconstructions remain difficult

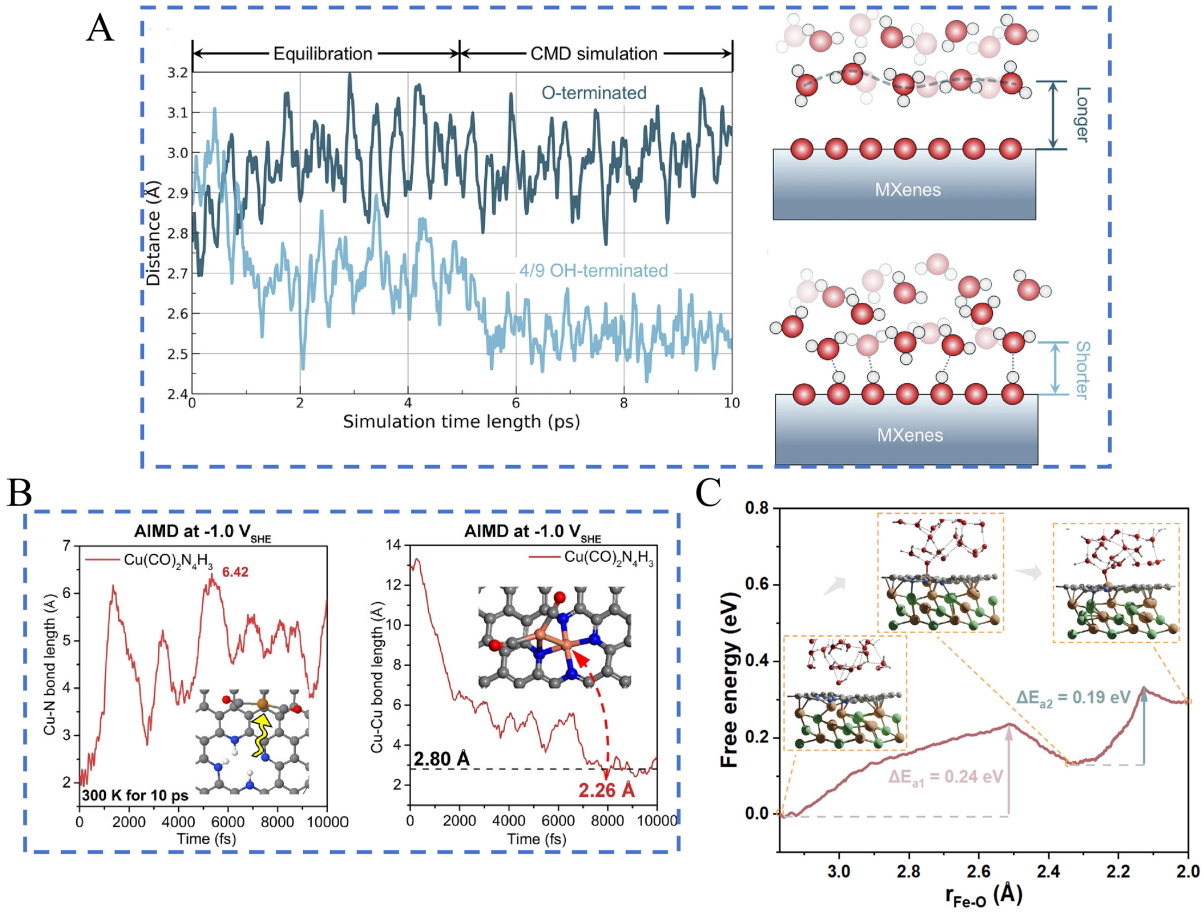


Figure 4. Catalytic activity revealed by CP-MD calculations. (A) Evolution of the interfacial water-surface distance and hydrogen-bond networks on O- and mixed O/OH-terminated Ti_2C MXenes. Adapted from reference[60] under CC BY 4.0 License; (B) Constant-potential AIMD trajectories showing Cu-N bond dissociation and subsequent Cu-Cu bond formation during the dynamic sintering of Cu-N-C catalysts. Adapted with permission from reference[61]. Copyright © 2024, Wiley-VCH GmbH; (C) Gibbs free energy diagram of the regeneration mechanism of Fe-N-C sites in NiFe alloys. Reproduced from reference[62] under CC BY 3.0 License. CP-MD: Constant-potential molecular dynamics; AIMD: ab initio molecular dynamics; CMD: constrained molecular dynamics.

to observe directly[63-65]. Conventional computational approaches, including static DFT and short-timescale AIMD, are also constrained by system size, accessible timescale and the difficulty of realistically describing electrochemical interfaces[66]. To address these limitations, recent efforts have increasingly turned to large-scale, long-timescale and constant-potential simulations of realistic electrochemical environments. In parallel, ML has emerged as a powerful data-driven tool and has driven a broader methodological shift in materials science and catalysis. In electrocatalysis, ML has been used primarily for high-throughput screening and performance prediction. By constructing feature spaces based on composition, crystal structure or fundamental physicochemical properties, researchers have established mappings between material descriptors and catalytic activity[67]. However, although purely data-driven black-box models can provide accurate predictions, they often obscure the physicochemical logic embedded in the data[68].

Given the growing range of computational and AI-assisted approaches in electrocatalysis, method selection should be guided by the scientific question and the required level of physical realism. Static DFT is generally suitable for analyzing intrinsic electronic structures, adsorption energetics, and elementary reaction barriers, whereas GC-DFT is more appropriate for potential-dependent charge states and energetics. AIMD or constant-potential MD is needed when explicit solvation, thermal fluctuations, or interfacial reconstruction is important, although these methods require greater computational resources and specialized expertise.

Table 1. Scope and applicability of computational and AI-assisted approaches across different catalytic microenvironment regimes

Approach	Most suitable scientific question	Main capability	Practical prerequisites and entry barriers	Major limitation
Static DFT[4,66,69]	Adsorption energies, electronic structure, elementary reaction energetics	High-accuracy electronic-structure analysis	Moderate; requires atomistic modeling and DFT expertise	Limited dynamics and interfacial fluctuations
GC-DFT[43,51,70]	Potential-dependent energetics and electronic response	Explicit treatment of electron exchange at fixed electron chemical potential	High; requires electrochemical thermodynamics and specialized implementations	High computational cost and limited system size
AIMD[60,71]	Solvation structure, hydrogen bonding, short-time interfacial dynamics	Explicit atomic dynamics with DFT accuracy	High computational cost	Limited spatial and temporal scales
Constant-potential MD[44,45,72]	Potential-dependent interfacial dynamics and electrode-electrolyte coupling	Dynamical response under controlled electrode potential	High; requires suitable constant-potential implementation/model	Computationally demanding and method dependent
Interpretable ML/symbolic regression[67,73,74]	Descriptor discovery and structure-property relationships	Fast prediction and interpretable correlations	Requires curated datasets and descriptor construction	Dataset dependence and limited extrapolation
NNP/ML potential[75-77]	Long-time and large-scale atomistic dynamics	Near-DFT accuracy at much lower computational cost	High initial cost for training-data generation and validation	Transferability and extrapolation uncertainty
LLMs[78-80]	Literature extraction, knowledge organization, semantic reasoning	Handles large volumes of unstructured information	Relatively low technical entry barrier	Hallucination and source-reliability issues
AI agent[15,81]	Multi-step workflow orchestration and tool integration	Connects literature, simulation, analysis, and experiments	High system-integration and validation requirements	Error propagation, tool-use reliability, and traceability

DFT: Density functional theory; GC-DFT: grand-canonical density functional theory; AIMD: ab initio molecular dynamics; MD: molecular dynamics; NNP: neural network potential; ML: machine learning; LLMs: large language models; AI: artificial intelligence.

For processes beyond the spatial and temporal scales accessible to first-principles dynamics, validated NNPs offer a more efficient alternative. Interpretable ML and symbolic regression are useful for descriptor discovery and large-scale screening when representative datasets are available. LLMs and AI agents can support knowledge integration and workflow orchestration, but require source verification and human oversight. In practice, these approaches can be combined in a tiered workflow, from low-cost screening to increasingly realistic simulations of selected systems. Their principal applications, entry barriers, and limitations are summarized in Table 1.

Therefore, the key challenge is not only to improve prediction accuracy, but also to extract physically meaningful descriptors that explain why specific structures exhibit superior activity. Unlike conventional black-box models, symbolic regression can automatically identify a small set of key physical quantities from a large pool of candidate features. It can then construct analytical expressions that approximate target properties, directly yielding chemically interpretable activity descriptors[82]. As shown in Figure 5A, Nair *et al.* demonstrated that sure independence screening and sparsifying operator (SISSO) can identify critical variables from diverse primary features[73]. SISSO can also build model ensembles through bootstrap resampling and feature dropout, thereby providing both mean predictions and uncertainty estimates. In that work, oxide stability under acidic OER conditions was selected as the target property. Through only 30 rounds of active learning, 12 acid-stable materials were identified from 1,470 candidate oxides. This result highlights the value of symbolic regression not only for mechanistic interpretation, but also for efficient screening and closed-loop discovery. Omidvar *et al.* developed a theory-infused neural network (TinNet) framework to examine the origin of surface reactivity in Pt monolayer core-shell catalysts for the ORR[83]. By integrating a graph neural network with the Newns-Anderson chemisorption model, TinNet links predictive accuracy to physically interpretable electronic descriptors. Shapley additive explanations (SHAP) analysis

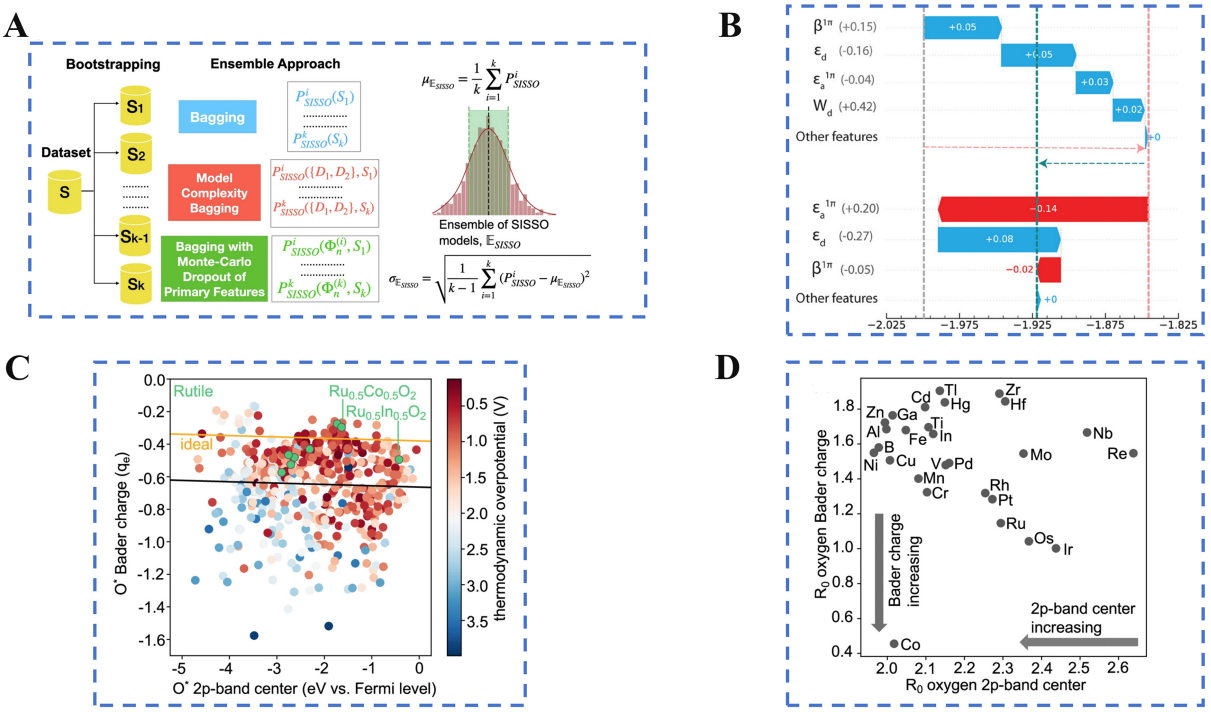


Figure 5. Interpretable machine learning for catalytic activity calculations. (A) Framework of the ensemble approach for the SISSO model. Reproduced from reference[73] under CC BY 4.0 License; (B) Local SHAP analysis of OH adsorption on Pt monolayer core-shell catalysts, revealing the contributions of key electronic factors to variations in adsorption strength. Adapted from reference[83] under the terms of the Creative Commons Attribution License; (C) Thermodynamic overpotential as a function of the adsorbed oxygen 2*p*-band center and Bader charge. Adapted from reference[84] under CC BY 4.0 License; (D) Fitted R_0 values for predicting oxygen Bader charge *vs.* those for predicting the oxygen 2*p*-band center as a function of neighboring metal species. Adapted from reference[84] under CC BY 4.0 License. SISSO: Sure independence screening and sparsifying operator; SHAP: Shapley additive explanations.

further decomposed variations in OH adsorption into contributions from individual electronic factors. As shown in Figure 5B, the enhanced ORR activity of Pt-based core-shell catalysts was attributed to the combined effects of the metal *d*-band center, the renormalized OH 1π resonance energy and the 1π-*d* coupling strength. These factors collectively regulate the occupation of adsorbate-metal antibonding states. The analysis further showed that OH binding cannot be explained solely by the conventional *d*-band-center descriptor, because sp-band-induced shifts in adsorbate resonance states also contribute substantially to chemisorption. This physics-informed and explainable ML framework therefore provides an interpretable connection between local alloy environments, electronic interactions and catalytic reactivity. Lunger *et al.* combined density functional theory with per-site graph neural networks and descriptor-based modeling to establish an atom-by-atom framework for understanding OER activity in multicomponent perovskite oxides[84]. Their dataset contained more than 20,000 substituted bulk perovskites and over 10,000 surface structures with O, OH and OOH* adsorption energies, enabling the local chemical environment to be linked with site-specific electronic properties. The ML models accurately predicted per-site properties including oxygen 2*p*-band center, metal *d*-band center and Bader charge directly from local atomic environments. A multi-linear model further revealed that the 2*p*-band center and Bader charge of adsorbed oxygen are the dominant descriptors governing OER intermediate binding energies. As shown in Figure 5C, these two independently tunable descriptors define a two-dimensional activity landscape in which variations in local electronic properties lead to substantial deviations from conventional OER scaling relationships, with theoretical overpotentials as low as 0.21 V predicted for selected perovskite surfaces. Figure 5D further maps the fitted bond-valence parameters associated with neighboring metal atoms, providing a direct strategy for tuning oxygen 2*p*-band center and Bader charge through compositional substitution. This framework demonstrates how ML can translate complex local chemical environments into physically interpretable descriptors and further guide atom-by-atom catalyst design.

This transition from black-box to white-box modeling is important for uncovering microscopic catalytic mechanisms. Unlike black-box approaches, which primarily fit input-output correlations, white-box models expose the underlying physicochemical relationships and provide transparent, interpretable and physically meaningful descriptions of catalytic behavior[85]. Such interpretability can move beyond the limited applicability of traditional single-descriptor frameworks in complex multiphase catalytic systems. It also enables more precise quantitative modeling of synergistic effects, coordination-environment engineering and strain-related effects, thereby providing actionable mechanistic insight for rational catalyst design.

In recent years, NNPs have advanced rapidly in electrocatalysis research. Owing to their high computational efficiency, NNP-based molecular dynamics can now be combined with enhanced sampling methods, such as umbrella sampling and metadynamics, to study explicit-solvent interfacial systems across larger spatial and temporal scales while retaining near-DFT accuracy[86]. This progress enables more reliable quantitative characterization of complex reaction pathways and free-energy landscapes. It also makes it possible to directly track the evolution of catalyst surface structures during reactions, providing insight into the dynamic nature of active sites under realistic operating conditions[87]. Despite this substantial expansion of accessible spatial and temporal scales, most current NNP models are still based on the constant-charge assumption. This assumption imposes clear limitations for describing real electrochemical systems. In practice, electrochemical reactions usually occur under constant-potential conditions, where the electron number dynamically adjusts in response to reaction progress and the interfacial environment. To bridge this gap, Chen *et al.* proposed a dual-learning NNP framework that incorporates electrode potential as an input variable to maintain a target potential during simulation[88]. However, such approaches remain thermodynamically incomplete with respect to the underlying physical ensemble, because the electron number is not treated as an independent degree of freedom participating in thermodynamic equilibrium. In a finite-size DFT/AIMD supercell, the potential should therefore not be regarded as an instantaneously fixed quantity. Instead, it is better understood as a thermodynamic variable that fluctuates around a target mean value. When the potential is used as an input parameter for a neural network, the thermal fluctuation channel of the interfacial potential around its mean is suppressed. Consequently, the potential is no longer spontaneously sampled according to the fluctuation-dissipation relation.

Building on these developments, Chen *et al.* developed a constant-potential reactor simulation framework that further extended machine-learning-based electrochemical simulations at the level of the underlying physical model[89]. As shown in Figure 6A, this work constructed a variable-charge neural network potential (veNNP) for the Au-water interface and integrated active learning, an explicit/implicit hybrid solvation model and CP-MD. This framework enabled nanosecond-scale simulations of Au(110)/Au(111)-water interfaces [Figure 6B], while retaining near-DFT accuracy for energies, forces and E_f. The simulations showed that, as the potential shifted negatively, electrons accumulated on the Au surface and preferentially localized at protruding surface sites. These sites more readily transferred electrons to CO_2 and induced CO_2 bending, thereby exhibiting higher catalytic activity. The study further clarified the role of K^+: rather than directly coordinating with CO_2 to promote activation, K^+ enhanced surface charge accumulation and stabilized the large dipole moment of activated CO_2, lowering the barriers for CO_2 adsorption and activation[89]. At the same time, K^+ disrupted the hydrogen-bond network of interfacial water and suppressed proton transport, thereby inhibiting the competing hydrogen evolution reaction (HER). From the perspective of dynamic interfaces, this work explains why alkali cations can promote CO_2 reduction while suppressing HER. Dufils *et al.* developed PiNNwall, a machine-learning-assisted framework for modeling chemically heterogeneous electrode-electrolyte interfaces under applied bias[90]. The framework integrates the atomistic machine-learning package PiNN with the constant-potential molecular-dynamics engine MetalWalls. Unlike chemically uniform perfect-metal electrode models, PiNNwall predicts the charge-response kernel and base charge distribution from the local atomic environment. These quantities are then

combined with the electrolyte-induced electrostatic potential to determine electrode-atom response charges dynamically during molecular dynamics simulations. As shown in Figure 6C, this workflow incorporates local geometry and chemical heterogeneity directly into the polarization response of the electrode. Applications to doped graphene and graphene oxide further showed that surface functional groups can substantially alter interfacial capacitance, ionic distributions and charge relaxation by modifying local polarizability and surface chemistry. PiNNwall therefore extends constant-potential simulations to chemically heterogeneous interfaces, where local structural and chemical microenvironments govern the interfacial charge response. Bergmann *et al.* developed Response Analysis in z-Orientation (RAZOR), a response-augmented machine-learning framework that extends conventional machine-learning interatomic potentials (MLIPs) to electrified solid-liquid interfaces under finite bias[91]. Rather than explicitly resolving the interfacial charge distribution at each step, RAZOR learns the work function as the first-order energetic response to an applied bias charge, while using the corresponding force response to stabilize the model. Combined with electronic capacitance, this treatment describes potential-dependent interfacial energetics up to second order while retaining the efficiency of short-range MLIPs. When applied to OH adsorption on Cu (100), RAZOR-MLIP molecular dynamics revealed pronounced charge-induced restructuring of the adsorbate configuration. As shown in Figure 6D, OH preferentially adopted a nearly parallel bridge configuration under negative surface charge, whereas positive charging stabilized an upright hollow-site configuration. This transition was accompanied by a substantial change in the interfacial work function. Transforming the constant-charge free energies to constant-potential conditions further reproduced the experimentally observed pH dependence of the preferred adsorption site. These results indicate that electrode charging can dynamically reshape local adsorption configurations, and that response-aware ML potentials provide an efficient route for resolving potential-dependent interfacial microenvironments.

The development of NNPs is moving theoretical electrocatalysis beyond static models and short-timescale approximations toward dynamic interfacial simulations under realistic operating conditions. By combining near-DFT accuracy with computational efficiency far exceeding that of AIMD, NNPs enable explicit-solvent interfaces, electrode surface reconstruction, complex reaction pathways and free-energy landscapes to be explored over extended time and length scales[75]. They therefore provide a powerful route for resolving the dynamic evolution of catalytic active sites during electrocatalytic processes. Nevertheless, constant-potential NNPs remain at an early stage. Major challenges persist in describing long-range electrostatics, interfacial polarization and charge redistribution, as well as in ensuring transferability across different potentials and surface states. Developing physically grounded and transferable constant-potential NNP frameworks will therefore be central to future progress in electrocatalysis simulations.

Although constant-potential NNPs greatly extend the spatial and temporal scales accessible to electrocatalytic simulations, they also produce increasingly complex mechanistic and configurational information. Such information is difficult to analyze systematically or integrate through conventional manual workflows. At the same time, the rapid expansion of electrocatalysis literature, simulation datasets and multimodal experimental data is making catalyst discovery increasingly dependent on automated knowledge extraction and cross-scale workflow coordination. In this context, closed-loop frameworks that integrate literature understanding, atomistic simulation, mechanistic analysis and experimental feedback are emerging as an important frontier for microenvironment-aware catalyst discovery. Rather than serving only as text-generation tools, LLMs are increasingly being explored as knowledge interfaces that can organize unstructured scientific information and connect semantic knowledge with computational workflows[78,92].

Exemplifying this approach, Hu *et al.* employed LLMs to automatically extract catalyst compositions, structural characteristics, reaction conditions, and performance metrics from large-scale literature datasets, thereby enabling a high-throughput analysis of catalyst structure-activity relationships[93]. By coupling a

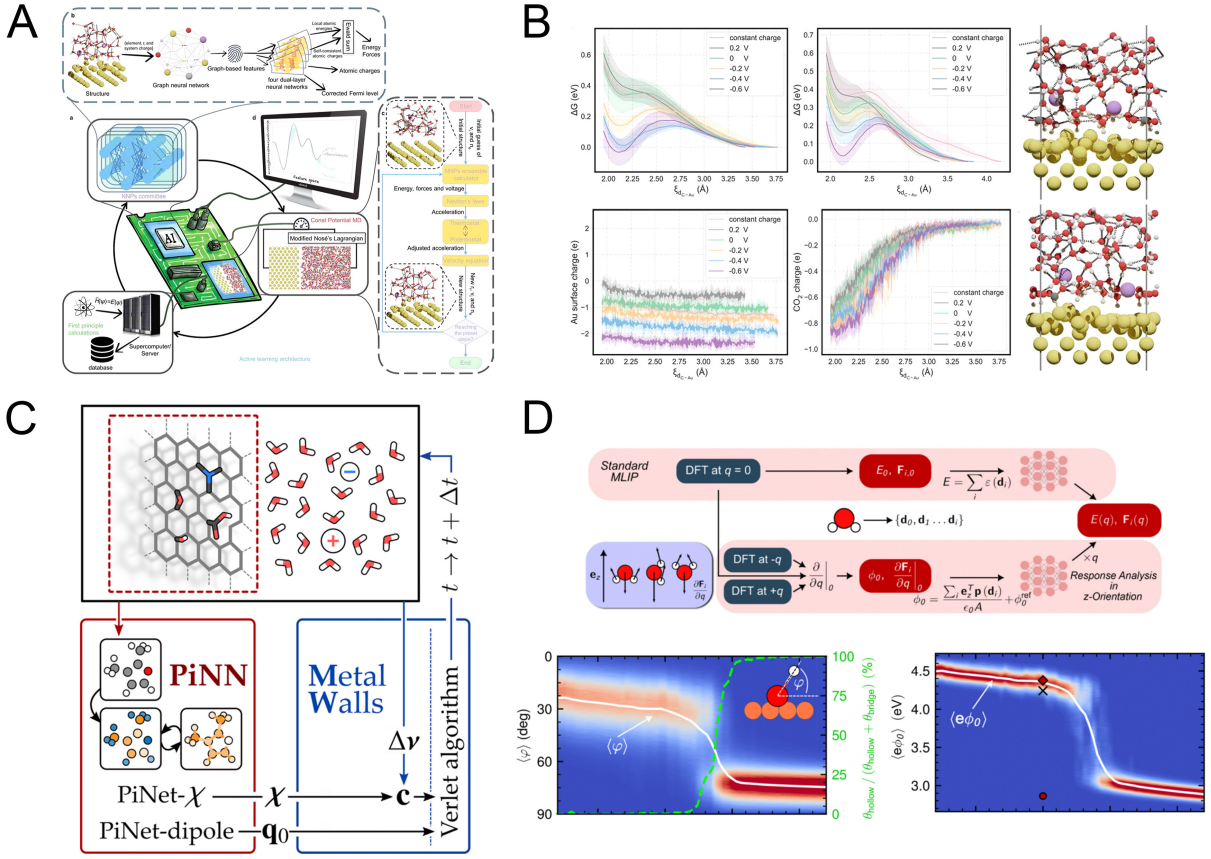


Figure 6. Diversity and application of constant-potential NNPs. (A) The active learning workflow for training a constant potential reactor NNP, which iteratively refines the potential by sampling high-uncertainty configurations. Reproduced from reference[89] under CC BY-NC-ND 4.0 License; (B) The potential-dependent free energy profiles for CO_2 adsorption at Au-water interfaces, as revealed by constant-potential MD simulations. Reproduced from reference[89] under CC BY-NC-ND 4.0 License; (C) PiNNwall framework coupling machine-learned charge-response kernels and base charges with constant-potential molecular dynamics for heterogeneous electrode-electrolyte interfaces. Reproduced from reference[90] under CC BY 4.0 License; (D) RAZOR framework and RAZOR-MLIP simulations of OH-covered Cu (100), illustrating charge-induced adsorption-site switching and the associated work-function response. Adapted from reference[91] under CC BY 4.0 License. MLIP: Machine-learning interatomic potential; DFT: density functional theory; MD: molecular dynamics; RAZOR: Response Analysis in z-Orientation.

random forest model with SHAP-based interpretability analysis to predict NH_3 yield, they revealed the critical roles of both intrinsic atomic properties and external microenvironmental factors, such as space-group number, electronegativity difference, electrolyte type, and weakly acidic pH, in determining eNRR performance [Figure 7A]. The study further used clustering analysis to resolve feature distributions among samples with different Faradaic efficiencies. The predictive model was then used to recommend and evaluate new catalyst systems through natural language. Among the candidates, Mo-W dual atoms supported on Ti_2NO_2 MXene were predicted to deliver both high NH_3 yield and high Faradaic efficiency, with their stability further validated by AIMD calculations[93]. This work illustrates how LLM-based frameworks can transform dispersed experimental literature into computable structure-performance knowledge. When combined with interpretable ML, such frameworks can help bridge microscopic catalyst features and macroscopic performance, providing a data-driven route for intelligent catalyst screening and rational design.

AI agents elevate LLMs from mere "language tools" to autonomous research entities capable of planning, decision-making, and invoking external tools to solve complex mechanistic puzzles. Operating with LLMs as their central cognitive engine, these agents can perceive their environment, decompose complex tasks, and

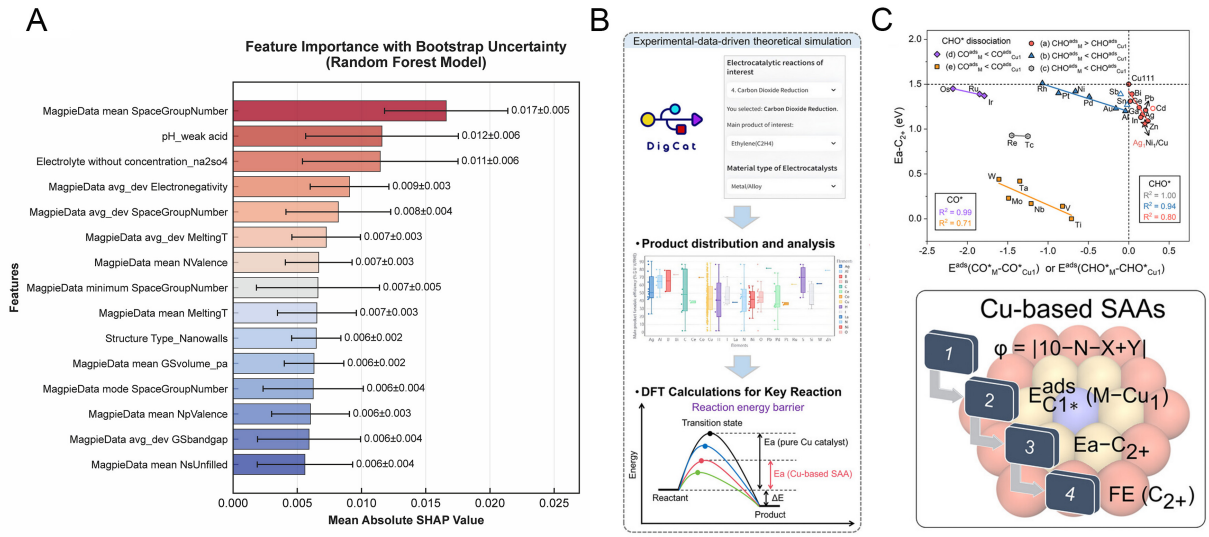


Figure 7. LLMs and AI agent for the microscopic mechanisms. (A) Mean absolute SHAP values for the most important features identified by the Random Forest model. Reproduced from reference[93] under CC BY 4.0 License; (B) The Catalysis AI Agent framework design. Reproduced from reference[94] under CC BY 4.0 License; (C) The energetic descriptor based on the adsorption-energy difference of CO or CHO between the dopant site (M) and the neighboring Cu1 site. Reproduced from reference[94] under CC BY 4.0 License. LLMs: Large language models; AI: artificial intelligence; SHAP: Shapley additive explanations; DFT: density functional theory; SAA: single-atom alloy.

interact with a wide range of tools, including information retrieval systems, code execution modules, database queries, machine-learning predictors, and automated experimental platforms[79]. In electrocatalysis, such capabilities could support collaborative "semantic reasoning-atomic simulation" frameworks that track and optimize the dynamic evolution of active sites under working conditions. Wang *et al.* developed a Catalysis AI Agent [Figure 7B] based on large-scale catalytic experimental data and LLMs[94]. The system was used to guide mechanistic analysis and targeted screening of Cu-based single-atom alloy catalysts for multicarbon product formation in electrochemical CO_2 reduction. By integrating experimental data with DFT calculations, the AI agent identified the classification of guest dopant metals as a key factor for establishing reliable structure-selectivity relationships[94]. It further introduced an energetic descriptor based on the CO or CHO adsorption-energy difference between the dopant site (*M*) and the neighboring Cu_1 site. This descriptor enabled classification of C-C coupling pathways and rate-determining energy barriers across different Cu-based single-atom alloys [Figure 7C]. The study also formulated a structural descriptor, φ, that links electronic-scale features, including periodic-table position, electronegativity and valence *d*-electron configuration, with the adsorption strength of C-C coupling precursors and the macroscopic Faradaic efficiency toward C_{2+} products. This descriptor explains the experimentally observed differences in C_{2+} selectivity caused by different dopant elements. It also predicts promising catalysts with high C_{2+} selectivity, including the dual-single-atom alloys Ni_1Zn_1/Cu and Rh_1Zn_1/Cu. Overall, this work illustrates how AI agents can organize catalysis research into a closed-loop workflow spanning data mining, mechanistic hypothesis generation, microscopic descriptor construction and candidate-material screening. Such workflows can accelerate the discovery of relationships among catalyst microstructure, reaction mechanism and macroscopic performance, providing an intelligent route for the rational design of high-performance electrocatalysts.

Applications of LLMs and AI agents specifically targeting catalytic microenvironments remain at an early stage compared with their more established use in catalyst discovery, property prediction, and active-site screening. Nevertheless, recent studies have begun to extend AI-assisted research toward the interpretation and regulation of local catalytic environments. Lin *et al.* employed reasoning language models within a

multi-agent framework to analyze surface-modified two-dimensional metal-organic layers for C-H activation[95]. By extracting interpretable rules from experimental data, the framework revealed how molecular modifiers regulate the local electronic environment and identified their electronic effects, rather than direct interactions with reaction intermediates, as a key origin of catalytic activity. More recently, Zhao *et al.* developed an AI-agent-guided strategy for nickel-based biomass electrooxidation[96], in which the agent identified Mn doping as a route to generate a built-in electric field that simultaneously modulates the electronic structure and interfacial microenvironment. By integrating *in situ* spectroscopic feedback with DFT and MD simulations, the agent further associated the enhanced catalytic behavior with disruption of the interfacial hydrogen-bond network and improved mass transport. These studies provide emerging evidence that AI-based systems can move beyond conventional catalyst screening toward microenvironment-aware mechanistic analysis and design. However, such applications remain relatively limited, and a mature, generally applicable capability for fully autonomous exploration and optimization of dynamically evolving catalytic microenvironments under realistic reaction conditions has yet to be established.

Despite these opportunities, the application of LLMs and AI agents in scientific research introduces several important risks that should be distinguished from those of conventional numerical models. First, LLM-generated statements may contain hallucinated, outdated, or insufficiently supported scientific information, making source verification essential for mechanistic interpretation. Second, in agent-based workflows, errors may originate not only from language-model reasoning but also from inappropriate tool selection, incorrect parameter settings, failed calculations, or inaccurate interpretation of computational outputs. Because multi-step agents sequentially connect literature retrieval, structure generation, simulation, and data analysis, such errors can propagate through the workflow and become increasingly difficult to identify. Third, the stochastic nature of LLM outputs and the heterogeneity of external tools can compromise reproducibility and traceability. Therefore, reliable scientific agents should incorporate source-grounded knowledge retrieval, structured tool interfaces, physicochemical constraints, uncertainty or consistency checks, complete workflow logging, and human validation at critical decision points. These safeguards are essential if LLMs and AI agents are to evolve from convenient research assistants into reliable components of mechanism-guided scientific discovery.

The continued development of LLMs and AI agents is moving electrocatalysis research beyond passive knowledge extraction and candidate recommendation toward active closed-loop optimization. In this context, automated experimental platforms serve as physical validation and feedback endpoints for virtual simulation loops. The integration of advanced software and hardware allows theoretical designs to be rapidly tested under realistic electrochemical conditions. It also accelerates the transition of electrocatalyst screening toward automated, closed-loop and intelligent discovery[97]. Fisker Bødker *et al.* reported the FastCat autonomous experimental platform, which integrates robotic synthesis, electrochemical testing, data analysis and Bayesian optimization[98]. This platform was used for the closed-loop discovery of platinum-group-metal-free multimetal layered double hydroxide (LDH) catalysts for the OER [Figure 8A]. By exploring a broad compositional space involving elements such as Cr, Fe, Co and Ni, FastCat identified several high-performance Ni-Fe-Cr-Co catalysts. The best-performing sample achieved an overpotential as low as 231 mV at 20 mA·cm^{-2}, outperforming the conventional NiFe-LDH benchmark catalyst. Beyond performance optimization, FastCat also revealed composition-activity relationships from high-throughput composition-performance datasets[98]. Catalysts with superior activity at high current densities were typically enriched in Fe and Ni, whereas Al, Mn, Cu and Zn contributed less substantially[98]. Some of these elements may even dissolve under alkaline OER conditions, reflecting the effects of LDH stoichiometric constraints, precursor dissolution and Ni-substrate leaching on active-phase formation[98]. This work shows that automated laboratories can rapidly establish composition-structure-performance relationships for multielement catalysts under conditions close to practical alkaline electrolysis. Such platforms can accelerate the

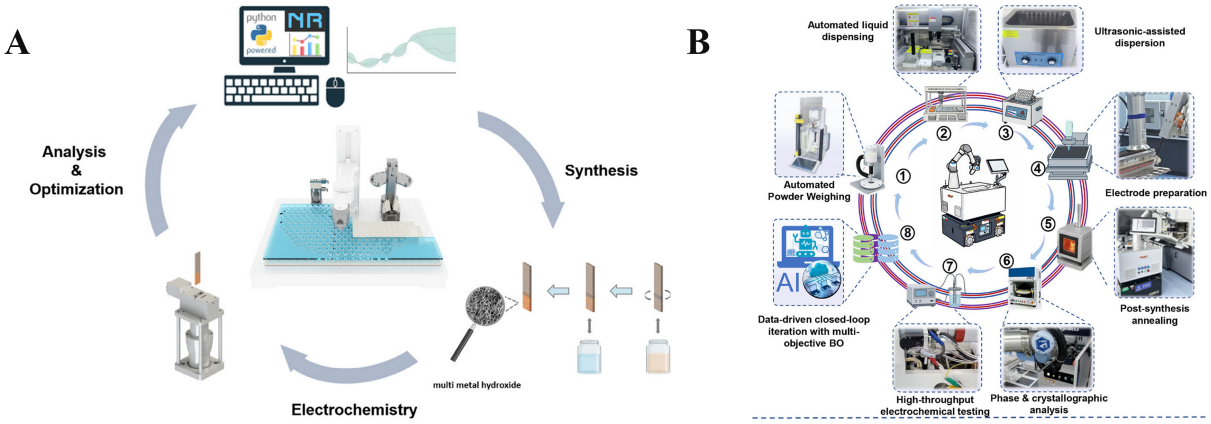


Figure 8. Autonomous experimental platforms for electrocatalyst discovery and optimization. (A) Schematic of the FastCat autonomous catalyst-development platform integrating robotic synthesis, electrochemical testing, data analysis, and closed-loop optimization. Reproduced from reference[98] under CC BY 4.0 License; (B) Automated robotic platform integrating high-throughput catalyst synthesis, structural characterization, electrochemical testing, and data-driven multi-objective Bayesian optimization for closed-loop discovery of high-entropy CER catalysts. Reproduced with permission from reference[99]. Copyright © 2026, Wiley-VCH GmbH. BO: Bayesian optimization.

identification of active components, stability assessment and candidate screening in complex catalytic systems. From the perspective of catalytic microenvironments, they become particularly valuable when compositional optimization is coupled with operando characterization. This integration allows experimentally observed activity trends to be linked to dynamically evolving active phases. Similarly, Yang *et al.* developed a closed-loop robotic AI-chemist platform for the autonomous discovery of high-entropy electrocatalysts for the chlorine evolution reaction[99]. The workflow integrates prior-knowledge extraction, robotic high-throughput synthesis, electrochemical testing and Pareto-guided multi-objective Bayesian optimization to explore the Ru-Cu-Ni-Cr-W compositional space. Rather than optimizing a single catalytic metric, the platform simultaneously considered catalytic activity, Cl_2 selectivity and material cost, allowing the search to progressively converge towards Pareto-optimal compositions [Figure 8B]. Starting from an initial library of 199 compositions, the Bayesian optimization loop refined the search space through five iterative rounds of targeted experiments and identified catalysts that balanced these competing objectives. SHAP analysis further revealed distinct elemental contributions to activity and selectivity: Ru and Cr promoted catalytic activity, whereas higher Ru contents tended to reduce Cl_2 selectivity. The optimized catalyst substantially reduced Ru loading while maintaining high activity and selectivity, and its performance was further validated in a solar-driven seawater electrolysis system.

To connect automated experimentation more directly with catalytic microenvironments, closed-loop platforms can treat microenvironment-related factors as controlled experimental variables and structured metadata. These factors include catalyst composition, synthesis parameters that regulate local coordination, electrolyte identity and concentration, pH, applied potential, temperature, and other operating conditions. Their effects can be monitored through operando characterization and linked to mechanistic descriptors obtained from DFT or molecular dynamics simulations, including active-site coordination, charge redistribution, adsorption energetics, interfacial solvation, and surface reconstruction. By integrating these variables and descriptors with measured catalytic performance, autonomous platforms can establish structure-microenvironment-mechanism-performance relationships rather than merely identify high-performing compositions.

Despite these advances, autonomous laboratories in electrocatalysis remain largely centered on catalyst synthesis, compositional screening, and the optimization of macroscopic performance metrics, whereas the systematic interrogation and control of catalytic microenvironments are still at an early stage. The recently

proposed AI-eChemist framework represents an initial step toward more microenvironment-aware autonomous experimentation by integrating high-throughput electrochemical measurements with multimodal operando characterization, data-driven analysis, and closed-loop decision-making. In particular, the joint analysis of electrochemical, spectroscopic, and product-distribution data offers a means of correlating catalyst composition and structural evolution with interfacial reaction processes and catalytic performance[100]. Such a "measurement-modeling-prediction-validation" workflow could enable autonomous platforms to progress beyond performance-oriented screening toward the identification, mechanistic interpretation, and ultimately rational optimization of dynamically evolving active-site and interfacial microenvironments. Nevertheless, this capability remains nascent, and fully autonomous closed-loop experimentation that directly treats catalytic microenvironment descriptors or variables as optimization targets has yet to become an established experimental paradigm.

In the future, electrocatalyst screening is expected to shift from passive strategies based on human experience and isolated models toward active closed-loop discovery. In this paradigm, LLMs can serve as knowledge interfaces, AI agents as execution cores and physicochemical constraints as the basis for reliability. For multi-objective optimization, complex-condition exploration and human-AI collaborative decision-making, the integration of LLMs and AI agents is likely to improve screening efficiency, expand the searchable chemical space and enhance the scalability of research workflows. However, the fidelity of AI predictions remains strongly constrained by the quality of the underlying datasets. Many current models are still optimized mainly for simplified thermodynamic descriptors, rather than realistic operating conditions involving solvation effects, applied potential and dynamic surface reconstruction. Progress toward efficient, reliable and transferable electrocatalyst discovery will therefore require advances in data standardization, model interpretability, multimodal integration, benchmark evaluation and deeper coupling with electrochemical mechanisms.

CONCLUSION AND OUTLOOK

This review highlights catalytic microenvironments as a unifying framework for understanding and designing electrocatalysts. Rather than treating activity as an intrinsic property of a static material, the evidence surveyed here indicates that it emerges from coupled local and operando factors. These factors include coordination structure, electronic states, interfacial interactions and their evolution under realistic reaction conditions. From this perspective, structural regulation defines the initial active-site microenvironment. Constant-potential and dynamic simulations reveal how this microenvironment evolves under operating conditions. Data-driven approaches, in turn, extract transferable relationships from increasingly complex structural and mechanistic information.

Future progress should focus less on expanding individual computational or AI tools in isolation and more on integrating them into microenvironment-aware workflows. Three directions are particularly important. First, operando characterization should be more tightly coupled with realistic interfacial simulations to identify the active-site states and transient microenvironments that govern catalytic reactions. Second, machine-learning models and NNPs need to become more transferable across electrode potentials, electrolyte compositions, surface states and reaction conditions, while retaining physical interpretability and uncertainty awareness. Third, AI agents and autonomous laboratories should move beyond catalyst-level screening toward closed-loop interrogation and control of catalytic microenvironments, in which experimentally or computationally measurable interfacial variables directly inform subsequent decisions. Achieving these goals will require standardized multimodal data, reliable mechanistic descriptors, transparent AI workflows and continuous validation between theory and experiment. Such integration may ultimately move electrocatalyst discovery from empirical optimization toward microenvironment-informed, mechanism-guided design under realistic operating conditions.

DECLARATIONS

Authors' contributions

Analyzed and interpreted the literature, prepared figures, and drafted the manuscript: Yu, X.
Revised the manuscript: Hu, X.; Chen, L.; Zhou, Z.
Provided supervision, revised the manuscript, and guided the overall structure: Chen, F.; Zhang, X.

Availability of data and materials

Not applicable.

AI and AI-assisted tools statement

During the preparation of this manuscript, the AI tool ChatGPT (OpenAI, version GPT-5.6 Sol, released 2026-07-09) was used to assist with language editing and improve readability. ChatGPT was also used to generate all individual graphical elements of the Graphical Abstract, including the dodecahedron, spheres, molecular structures, robot, robotic arm and conical flask. The authors subsequently arranged, edited and assembled these AI-generated elements using Microsoft PowerPoint to create the final Graphical Abstract. The tool did not influence the study design, data collection, analysis, interpretation, or the scientific content of the work. All authors take full responsibility for the accuracy, integrity, and final content of the manuscript.

Financial support and sponsorship

This work was supported by the National Natural Science Foundation of China (22573097) and the Natural Science Foundation of Henan Province (242300421129).

Conflicts of interest

Zhou, Z. is an Editorial Board Member of the journal *AI Agent*. Zhou, Z. was not involved in any steps of editorial processing, notably including reviewer selection, manuscript handling, and decision-making, while the other authors have declared that they have no conflicts of interest.

Ethical approval and consent to participate

Not applicable.

Consent for publication

Not applicable.

Copyright

© The Author(s) 2026.

REFERENCES

1. Chu, S.; Cui, Y.; Liu, N. The path towards sustainable energy. *Nat. Mater.* **2016**, *16*, 16-22. DOI PubMed
2. De La Peña, L.; Guo, R.; Cao, X.; Ni, X.; Zhang, W. Accelerating the energy transition to achieve carbon neutrality. *Resour. Conserv. Recycl.* **2022**, *177*, 105957. DOI
3. Gao, D.; Li, H.; Wei, P.; Wang, Y.; Wang, G.; Bao, X. Electrochemical synthesis of catalytic materials for energy catalysis. *Chin. J. Catal.* **2022**, *43*, 1001-16. DOI
4. Ling, C.; Cui, Y.; Lu, S.; Bai, X.; Wang, J. How computations accelerate electrocatalyst discovery. *Chem* **2022**, *8*, 1575-610. DOI
5. Centi, G.; Perathoner, S. Electrocatalysis: prospects and role to enable an E-chemistry future. *Chem. Rec.* **2025**, *25*, e202400259. DOI PubMed
6. Seifitokaldani, A.; Gabardo, C. M.; Burdyny, T.; et al. Hydronium-induced switching between CO_2 electroreduction pathways. *J. Am. Chem. Soc.* **2018**, *140*, 3833-7. DOI PubMed
7. Li, Y.; Wang, X.; Wang, Y.; et al. The decisive role of adsorbed OH* in low-potential CO electro-oxidation on single-atom catalytic sites. *Carbon. Energy.* **2023**, *5*, e310. DOI
8. He, R.; Wang, S.; Yang, L.; et al. Active site switching on high entropy phosphides as bifunctional oxygen electrocatalysts for rechargeable/robust Zn-air battery. *Energy. Environ. Sci.* **2024**, *17*, 7193-208. DOI

9. Wu, H.; Singh-Morgan, A.; Qi, K.; Zeng, Z.; Mougel, V.; Voiry, D. Electrocatalyst microenvironment engineering for enhanced product selectivity in carbon dioxide and nitrogen reduction reactions. *ACS. Catal.* **2023**, *13*, 5375-96. DOI PubMed PMC
10. Gasteiger, H. A.; Kocha, S. S.; Sompalli, B.; Wagner, F. T. Activity benchmarks and requirements for Pt, Pt-alloy, and non-Pt oxygen reduction catalysts for PEMFCs. *Appl. Catal. B. Environ.* **2005**, *56*, 9-35. DOI
11. Kibsgaard, J.; Chorkendorff, I. Considerations for the scaling-up of water splitting catalysts. *Nat. Energy.* **2019**, *4*, 430-3. DOI
12. Fernández-Vidal, J.; Koper, M. T. The role of surface science in electrocatalysis. *ACS. Catal.* **2026**, *16*, 2925-34. DOI PubMed PMC
13. Fabbri, E.; Nachtegaal, M.; Binninger, T.; et al. Dynamic surface self-reconstruction is the key of highly active perovskite nano-electrocatalysts for water splitting. *Nat. Mater.* **2017**, *16*, 925-31. DOI PubMed
14. Szymanski, N. J.; Rendy, B.; Fei, Y.; et al. An autonomous laboratory for the accelerated synthesis of inorganic materials. *Nature* **2023**, *624*, 86-91. DOI PubMed PMC
15. Boiko, D. A.; Macknight, R.; Kline, B.; Gomes, G. Autonomous chemical research with large language models. *Nature* **2023**, *624*, 570-8. DOI PubMed PMC
16. Zuo, X.; Yan, R.; Zhao, L.; et al. A hollow PdCuMoNiCo high-entropy alloy as an efficient bi-functional electrocatalyst for oxygen reduction and formic acid oxidation. *J. Mater. Chem. A.* **2022**, *10*, 14857-65. DOI
17. Ma, X.; Liu, H.; Yang, W.; Mao, G.; Zheng, L.; Jiang, H. L. Modulating coordination environment of single-atom catalysts and their proximity to photosensitive units for boosting MOF photocatalysis. *J. Am. Chem. Soc.* **2021**, *143*, 12220-9. DOI PubMed
18. Hammer, B.; Norskov, J. K. Why gold is the noblest of all the metals. *Nature* **1995**, *376*, 238-40. DOI
19. Greiner, M. T.; Jones, T. E.; Beeg, S.; et al. Free-atom-like d states in single-atom alloy catalysts. *Nat. Chem.* **2018**, *10*, 1008-15. DOI PubMed
20. Wang, S.; Pillai, H. S.; Xin, H. Bayesian learning of chemisorption for bridging the complexity of electronic descriptors. *Nat. Commun.* **2020**, *11*, 6132. DOI PubMed PMC
21. Saini, S.; Halldin Stenlid, J.; Abild-Pedersen, F. Electronic structure factors and the importance of adsorbate effects in chemisorption on surface alloys. *npj. Comput. Mater.* **2022**, *8*, 163. DOI
22. Kumar, A.; Tüysüz, H. Modulating local coordination in single-atom catalysts: from fundamental concepts to emerging breakthroughs in electrocatalysis. *Angew. Chem. Int. Ed. Engl.* **2026**, *65*, e3059499. DOI PubMed PMC
23. Chen, C.; Jin, H.; Wang, P.; et al. Local reaction environment in electrocatalysis. *Chem. Soc. Rev.* **2024**, *53*, 2022-55. DOI PubMed
24. Li, R.; Ma, W.; Liu, Y.; Zhang, L.; Zhou, Z. Towards sustainable electrochemical ammonia synthesis. *J. Mater. Chem. A.* **2023**, *11*, 18626-45. DOI
25. Parsa, S. M.; Miraboutalebi, S. M. R.; Shoeibi, S.; et al. Advances on multi-heteroatom doped carbon catalysts: synthesis, mechanistic insight, synergies, and application in microbial electrochemical energy, fuel and chemical production. *Carbon* **2026**, *251*, 121315. DOI
26. Yang, J.; Deng, L.; Wu, Y.; Peng, S. Charge state evolution in electrocatalysts for bridging the activity-stability gap in acidic oxygen evolution. *Acc. Chem. Res.* **2026**, *59*, 838-48. DOI PubMed
27. Ma, W.; Yao, J.; Xie, F.; et al. Optimizing electronic structure through point defect engineering for enhanced electrocatalytic energy conversion. *Green. Energy. Environ.* **2025**, *10*, 109-31. DOI
28. Wang, Y.; Huang, H.; Wu, J.; et al. Charge-polarized selenium vacancy in nickel diselenide enabling efficient and stable electrocatalytic conversion of oxygen to hydrogen peroxide. *Adv. Sci.* **2023**, *10*, 2205347. DOI PubMed PMC
29. Ling, T.; Yan, D. Y.; Jiao, Y.; et al. Engineering surface atomic structure of single-crystal cobalt (II) oxide nanorods for superior electrocatalysis. *Nat. Commun.* **2016**, *7*, 12876. DOI PubMed PMC
30. Zhang, Y.; Chen, D.; Yu, S.; Feng, Y.; Zhang, C.; Hu, J. Al-induced local coordination engineering of Ni: steering the two-electron oxygen reduction process. *Adv. Funct. Mater.* **2025**, *35*, e13626. DOI
31. Gao, X.; Huang, G.; Jing, S.; et al. Strategies for enhancing catalytic performance of single-atom catalysts in 2e$^-$ oxygen reduction reaction: a review. *The. Innovation. Mater.* **2025**, *3*, 100141. DOI
32. Xue, D.; Zhao, Y.; Cao, J.; Wang, Y.; Li, X.; Ma, T. Spin engineering of dual-atom site catalysts for efficient electrochemical energy conversion. *Adv. Mater.* **2025**, *37*, 2504213. DOI PubMed PMC
33. Luo, B. Y.; Li, C.; Yang, Y. M.; Du, W.; Wang, Y. M. Impact of halogen axial coordination on the electronic and magnetic properties of MN_4 single-atom catalysts for oxygen reduction. *Phys. Chem. Chem. Phys.* **2026**, *28*, 4188-93. DOI PubMed
34. Zeng, R.; Li, Y.; Wan, Q.; et al. Orbital coupling of dual-atom sites boosts electrocatalytic NO oxidation and dynamic intracellular response. *Adv. Mater.* **2025**, *37*, 2416371. DOI PubMed
35. Cao, L.; Huang, J.; Wu, X.; et al. Active-site stabilized Bi metal-organic framework-based catalyst for highly active and selective electroreduction of CO_2 to formate over a wide potential window. *Nanoscale* **2023**, *15*, 19522-32. DOI PubMed
36. Hao, J.; Wu, K.; Lyu, C.; et al. Recent advances in interface engineering of Fe/Co/Ni-based heterostructure electrocatalysts for water splitting. *Mater. Horiz.* **2023**, *10*, 2312-42. DOI PubMed

37. Zhao, X.; Liu, M.; Wang, Y.; et al. Designing a built-in electric field for efficient energy electrocatalysis. *ACS. Nano.* **2022**, *16*, 19959-79. DOI PubMed
38. Wang, K.; Shen, Z.; Qi, F.; Yuan, Y.; Xiao, C.; Pan, H. Recent advances in built-in electric field for efficient energy electrocatalysis. *Carbon. Neutralization.* **2025**, *4*, e70029. DOI
39. Nwaji, N.; Fikadu, B.; Osial, M.; et al. Advanced functional $NiCo_2S_4$@$CoMo_2S_4$ heterojunction couple as electrode for hydrogen production via energy-saving urea oxidation. *Small* **2025**, *21*, 2410848. DOI PubMed
40. Yang, L.; Liu, H.; Li, Y.; et al. Customizing bonding affinity with multi-intermediates via interfacial electron capture to boost hydrogen evolution in alkaline water electrolysis. *Angew. Chem. Int. Ed. Engl.* **2024**, *64*, e202414518. DOI PubMed
41. Hammes-Schiffer, S. Proton-coupled electron transfer: moving together and charging forward. *J. Am. Chem. Soc.* **2015**, *137*, 8860-71. DOI PubMed PMC
42. Zhao, Q.; Martirez, J. M. P.; Carter, E. A. Revisiting understanding of electrochemical CO_2 reduction on Cu(111): competing proton-coupled electron transfer reaction mechanisms revealed by embedded correlated wavefunction theory. *J. Am. Chem. Soc.* **2021**, *143*, 6152-64. DOI PubMed
43. Sundararaman, R.; Goddard, W. A.; Arias, T. A. Grand canonical electronic density-functional theory: algorithms and applications to electrochemistry. *J. Chem. Phys.* **2017**, *146*, 114104. DOI PubMed
44. Bonnet, N.; Morishita, T.; Sugino, O.; Otani, M. First-principles molecular dynamics at a constant electrode potential. *Phys. Rev. Lett.* **2012**, *109*, 266101. DOI PubMed
45. Reed, S. K.; Lanning, O. J.; Madden, P. A. Electrochemical interface between an ionic liquid and a model metallic electrode. *J. Chem. Phys.* **2007**, *126*, 084704. DOI PubMed
46. Sundararaman, R.; Vigil-Fowler, D.; Schwarz, K. Improving the accuracy of atomistic simulations of the electrochemical interface. *Chem. Rev.* **2022**, *122*, 10651-74. DOI PubMed PMC
47. Ringe, S.; Hörmann, N. G.; Oberhofer, H.; Reuter, K. Implicit solvation methods for catalysis at electrified interfaces. *Chem. Rev.* **2022**, *122*, 10777-820. DOI PubMed PMC
48. Melander, M. M.; Wu, T.; Weckman, T.; Honkala, K. Constant inner potential DFT for modelling electrochemical systems under constant potential and bias. *npj. Comput. Mater.* **2024**, *10*, 5. DOI
49. Zhang, X.; Chen, J.; Wang, H.; et al. Dynamic structural evolution of single-atom catalysts at the catalyst-electrolyte interface: insights from electrochemical coupled field. *Nano. Lett.* **2025**, *25*, 6332-9. DOI PubMed
50. Cheng, D.; Wei, Z.; Zhang, Z.; Broekmann, P.; Alexandrova, A. N.; Sautet, P. Restructuring and activation of Cu(111) under electrocatalytic reduction conditions. *Angew. Chem. Int. Ed. Engl.* **2023**, *62*, e202218575. DOI PubMed
51. Hörmann, N. G.; Beinlich, S. D.; Reuter, K. Converging divergent paths: constant charge vs constant potential energetics in computational electrochemistry. *J. Phys. Chem. C.* **2024**, *128*, 5524-31. DOI
52. Yang, W.; Jia, Z.; Zhou, B.; Wei, L.; Gao, Z.; Li, H. Surface states of dual-atom catalysts should be considered for analysis of electrocatalytic activity. *Commun. Chem.* **2023**, *6*, 6. DOI PubMed PMC
53. Li, Y.; Lu, L.; Hu, K.; et al. Scalable and customizable single-atom coatings for pH-universal H_2O_2 electrosynthesis. *Adv. Mater.* **2026**, *38*, e21237. DOI PubMed PMC
54. Mathew, K.; Kolluru, V. S. C.; Mula, S.; Steinmann, S. N.; Hennig, R. G. Implicit self-consistent electrolyte model in plane-wave density-functional theory. *J. Chem. Phys.* **2019**, *151*, 234101. DOI PubMed
55. Liu, T.; Wang, Y.; Li, Y. Two-dimensional organometallic frameworks with pyridinic single-metal-atom sites for bifunctional ORR/OER. *Adv. Funct. Mater.* **2022**, *32*, 2207110. DOI
56. Zhao, X.; Liu, Y. Origin of selective production of hydrogen peroxide by electrochemical oxygen reduction. *J. Am. Chem. Soc.* **2021**, *143*, 9423-8. DOI PubMed
57. Yu, S.; Levell, Z.; Jiang, Z.; Zhao, X.; Liu, Y. What is the rate-limiting step of oxygen reduction reaction on Fe-N-C catalysts? *J. Am. Chem. Soc.* **2023**, *145*, 25352-6. DOI PubMed
58. Yue, J.; Li, Y.; Yang, C.; Luo, W. Hydroxyl-binding induced hydrogen bond network connectivity on Ru-based catalysts for efficient alkaline hydrogen oxidation electrocatalysis. *Angew. Chem. Int. Ed. Engl.* **2025**, *64*, e202415447. DOI PubMed
59. Wu, J.; Zhang, J.; Chen, M.; Yan, J.; Mao, B.; Feng, G. Regulating the electrical double layer to prevent water electrolysis for wet ionic liquids with cheap salts. *Nanoscale* **2023**, *15*, 18603-12. DOI PubMed
60. Chen, L.; Rosen, J.; Björk, J. Tuned interfacial hydrogen bonds for enhanced H_2 electrocatalysis kinetics on Ti_2C MXenes. *Commun. Chem.* **2026**, *9*, 246. DOI PubMed PMC
61. Qin, Y.; Zhao, W.; Xia, C.; et al. CO Intermediate-assisted dynamic Cu sintering during electrocatalytic CO_2 reduction on Cu-N-C catalysts. *Angew. Chem. Int. Ed. Engl.* **2024**, *63*, e202404763. DOI PubMed

62. Xue, Y.; Chen, L.; Zhang, L.; Zheng, G.; Zhang, X.; Zhou, Z. Activity and stability origin of core-shell catalysts: unignorable atomic diffusion behavior. *Chem. Sci.* **2025**, *16*, 3323-8. DOI PubMed PMC
63. Hasa, B.; Zhao, Y.; Jiao, F. In situ/operando characterization techniques of electrochemical CO_2 reduction. *Annu. Rev. Chem. Biomol. Eng.* **2023**, *14*, 165-85. DOI PubMed
64. Shen, W.; Ye, Y.; Xia, Q.; Xi, P. Progress in *in situ* characterization of electrocatalysis. *EES. Catal.* **2025**, *3*, 10-31. DOI
65. Olajide, G.; Maxson, T.; Szilvási, T. Temporal resolution of *in situ* TEM limits the characterization of catalyst site dynamics. *ACS. Catal.* **2025**, *15*, 18908-16. DOI
66. Schwarz, K.; Sundararaman, R. The electrochemical interface in first-principles calculations. *Surf. Sci. Rep.* **2020**, *75*, 100492. DOI PubMed PMC
67. Wu, H.; Chen, M.; Cheng, H.; Yang, T.; Zeng, M.; Yang, M. Interpretable physics-informed machine learning approaches to accelerate electrocatalyst development. *J. Mater. Inf.* **2025**, *5*, 15. DOI
68. Xu, L.; Zhou, J.; Bandarenka, A. S.; Chen, Z. Data-driven electrocatalyst discovery: recent trends in machine learning approaches and descriptor-based design principles. *Acc. Mater. Res.* **2026**, *7*, 294-308. DOI
69. Nørskov, J. K.; Rossmeisl, J.; Logadottir, A.; et al. Origin of the overpotential for oxygen reduction at a fuel-cell cathode. *J. Phys. Chem. B.* **2004**, *108*, 17886-92. DOI PubMed
70. Xia, Z.; Xiao, H. Grand canonical ensemble modeling of electrochemical interfaces made simple. *J. Chem. Theory. Comput.* **2023**, *19*, 5168-75. DOI PubMed
71. Groß, A. Challenges for ab initio molecular dynamics simulations of electrochemical interfaces. *Curr. Opin. Electrochem.* **2023**, *40*, 101345. DOI
72. Yu, L.; Chen, X.; Yao, N.; Gao, Y.; Zhang, Q. Constant-potential molecular dynamics simulation and its application in rechargeable batteries. *J. Mater. Chem. A.* **2023**, *11*, 11078-88. DOI
73. Nair, A. S.; Foppa, L.; Scheffler, M. Materials-discovery workflow guided by symbolic regression for identifying acid-stable oxides for electrocatalysis. *npj. Comput. Mater.* **2025**, *11*, 150. DOI
74. Ouyang, R.; Curtarolo, S.; Ahmetcik, E.; Scheffler, M.; Ghiringhelli, L. M. SISSO: a compressed-sensing method for identifying the best low-dimensional descriptor in an immensity of offered candidates. *Phys. Rev. Mater.* **2018**, *2*, 083802. DOI
75. Kocer, E.; Ko, T. W.; Behler, J. Neural network potentials: a concise overview of methods. *Annu. Rev. Phys. Chem.* **2022**, *73*, 163-86. DOI PubMed
76. Batzner, S.; Musaelian, A.; Sun, L.; et al. E(3)-equivariant graph neural networks for data-efficient and accurate interatomic potentials. *Nat. Commun.* **2022**, *13*, 2453. DOI PubMed PMC
77. Kulichenko, M.; Nebgen, B.; Lubbers, N.; et al. Data Generation for machine learning interatomic potentials and beyond. *Chem. Rev.* **2024**, *124*, 13681-714. DOI PubMed PMC
78. Choi, J.; Lee, B. Accelerating materials language processing with large language models. *Commun. Mater.* **2024**, *5*, 13. DOI
79. Ramos, M. C.; Collison, C. J.; White, A. D. A review of large language models and autonomous agents in chemistry. *Chem. Sci.* **2025**, *16*, 2514-72. DOI PubMed PMC
80. Mirza, A.; Alampara, N.; Kunchapu, S.; et al. A framework for evaluating the chemical knowledge and reasoning abilities of large language models against the expertise of chemists. *Nat. Chem.* **2025**, *17*, 1027-34. DOI PubMed PMC
81. Bran, A. M.; Cox, S.; Schilter, O.; Baldassari, C.; White, A. D.; Schwaller, P. Augmenting large language models with chemistry tools. *Nat. Mach. Intell.* **2024**, *6*, 525-35. DOI PubMed PMC
82. Wang, S. H.; Pillai, H. S.; Wang, S.; Achenie, L. E. K.; Xin, H. Infusing theory into deep learning for interpretable reactivity prediction. *Nat. Commun.* **2021**, *12*, 5288. DOI PubMed PMC
83. Omidvar, N.; Wang, S. H.; Huang, Y.; et al. Explainable AI for optimizing oxygen reduction on Pt monolayer core-shell catalysts. *Electrochem. Sci. Adv.* **2024**, *4*, e202300028. DOI
84. Lunger, J. R.; Karaguesian, J.; Chun, H.; et al. Towards atom-level understanding of metal oxide catalysts for the oxygen evolution reaction with machine learning. *npj. Comput. Mater.* **2024**, *10*, 80. DOI
85. Wellawatte, G. P.; Schwaller, P. Human interpretable structure-property relationships in chemistry using explainable machine learning and large language models. *Commun. Chem.* **2025**, *8*, 11. DOI PubMed PMC
86. Li, Q.; Ouyang, Y.; Lu, S.; et al. Perspective on theoretical methods and modeling relating to electro-catalysis processes. *Chem. Commun.* **2020**, *56*, 9937-49. DOI PubMed
87. Bonati, L.; Polino, D.; Pizzolitto, C.; et al. The role of dynamics in heterogeneous catalysis: Surface diffusivity and N_2 decomposition on Fe(111). *Proc. Natl. Acad. Sci. U. S. A.* **2023**, *120*, e2313023120. DOI PubMed PMC
88. Chen, X.; El Khatib, M.; Lindgren, P.; Willard, A.; Medford, A. J.; Peterson, A. A. Atomistic learning in the electronically grand-canonical ensemble. *npj. Comput. Mater.* **2023**, *9*, 73. DOI

89. Chen, L.; Tian, Y.; Hu, X.; et al. Constant-potential MD with neural network potentials reveals cation effects on CO_2 reduction at Au-water interfaces. *JACS. Au.* **2025**, *6*, 868-80. DOI PubMed PMC
90. Dufils, T.; Knijff, L.; Shao, Y.; Zhang, C. PiNNwall: heterogeneous electrode models from integrating machine learning and atomistic simulation. *J. Chem. Theory. Comput.* **2023**, *19*, 5199-209. DOI PubMed PMC
91. Bergmann, N.; Bonnet, N.; Marzari, N.; Reuter, K.; Hörmann, N. G. Machine learning the energetics of electrified solid-liquid interfaces. *Phys. Rev. Lett.* **2025**, *135*, 146201. DOI PubMed
92. Hu, X.; Chen, L.; Wang, H.; Zhang, X.; Zhou, Z. Accelerating discovery in computational electrocatalysis: From machine learning potentials to AI-driven workflows. *Curr. Opin. Electrochem.* **2026**, *57*, 101848. DOI
93. Hu, X.; Chen, S.; Chen, L.; Wang, H.; Zhang, X.; Zhou, Z. Automating structure-activity analysis for electrochemical nitrogen reduction catalyst design through multi-agent collaborations. *Natl. Sci. Rev.* **2025**, *12*, nwaf372. DOI PubMed PMC
94. Wang, X.; Li, Z.; Zhang, D.; Li, H.; Xu, H.; Cheng, D. Catalysis AI agent guides discovering the universal design principle of Cu-based single-atom alloy catalysts for CO_2 electroreduction. *Angew. Chem. Int. Ed. Engl.* **2026**, *65*, e24612. DOI PubMed PMC
95. Lin, H.; Cui, X.; Dai, B.; et al. Reasoning language model as rule finder: a case study on C-H bond activation using 2D metal-organic frameworks. *ACS. Cent. Sci.* **2025**, *11*, 1135-46. DOI PubMed PMC
96. Zhao, P.; Zhang, Y.; Chen, B.; et al. AI-agent-guided design of dual-scale modulated nickel-based catalyst with built-in electric field for enhanced biomass electrooxidation. *ACS. Nano.* **2026**, *20*, 10640-50. DOI PubMed
97. Steinmann, S. N.; Hermawan, A.; Bin Jassar, M.; Seh, Z. W. Autonomous high-throughput computations in catalysis. *Chem. Catalysis.* **2022**, *2*, 940-56. DOI
98. Fisker Bødker, N.; Moretti, E. R.; Chang, J. H.; Vegge, T. FastCat: autonomous discovery of multielement layered double hydroxide alloy catalysts for alkaline oxygen evolution reaction. *Adv. Intell. Discov.* **2025**, *2*, e202500138. DOI
99. Yang, R.; Zhou, D.; Jia, Z.; et al. Toward practical design of high-entropy catalysts for chlorine evolution reaction via pareto-guided multi-objective bayesian optimization enabled by a robotic AI-chemist. *Angew. Chem. Int. Ed.* **2026**, *65*, e8794274. DOI
100. Tan, Y.; Chen, L.; Shan, X.; et al. Development of AI-*e*Chemist Laboratory. *AI. Agent.* **2026**, *2*, 17. DOI

Disclaimer/Publisher's Note: All statements, opinions, and data contained in this publication are solely those of the individual author(s) and contributor(s) and do not necessarily reflect those of OAE and/or the editor(s). OAE and/or the editor(s) disclaim any responsibility for harm to persons or property resulting from the use of any ideas, methods, instructions, or products mentioned in the content.

© The Author(s) 2026. Open Access This article is licensed under a Creative Commons Attribution 4.0 International License (https://creativecommons.org/licenses/by/4.0/), which permits unrestricted use, sharing, adaptation, distribution and reproduction in any medium or format, for any purpose, even commercially, as long as you give appropriate credit to the original author(s) and the source, provide a link to the Creative Commons license, and indicate if changes were made.